Please do not remove this page

Additive Manufacturing of Short Fiber Reinforced Thermoset Composites

Nawafleh, Nashat Mohammad Ibrahim

https://scholarship.miami.edu/esploro/outputs/doctoral/Additive-Manufacturing-of-Short-Fiber-Reinforced/991031453886202976/filesAndLinks?index=0

Nawafleh, N. M. I. (2020). Additive Manufacturing of Short Fiber Reinforced Thermoset Composites [University of Miami]. https://scholarship.miami.edu/esploro/outputs/doctoral/Additive-Manufacturing-of-Short-Fiber-Reinforced/991031453886202976

Free to read
Downloaded On 2024/04/29 17:13:47 -0400

Please do not remove this page

UNIVERSITY OF MIAMI

ADDITIVE MANUFACTURING OF SHORT FIBER REINFORCED THERMOSET COMPOSITES

By
Nashat Mohammad Ibrahim Nawafleh

A DISSERTATION

Submitted to the Faculty
of the University of Miami
in partial fulfillment of the requirements for
the degree of Doctor of Philosophy

Coral Gables, Florida

May 2020

©2020
Nashat Mohammad Ibrahim Nawafleh
All Rights Reserved

UNIVERSITY OF MIAMI

A dissertation submitted in partial fulfillment of
the requirements for the degree of
Doctor of Philosophy

ADDITIVE MANUFACTURING OF SHORT FIBER REINFORCED THERMOSET COMPOSITES

Nashat Mohammad Ibrahim Nawafleh

Approved:

_____ Emrah Celik, Ph.D. Assistant Professor of Mechanical Engineering	_____ Ryan Lee Karkkainen, Ph.D. Assistant Professor of Mechanical Engineering
_____ James Coakley, Ph.D. Assistant Professor of Mechanical Engineering	_____ Guillermo Prado, Ph.D. Dean of the Graduate School

_____
Edward Dauer, Ph.D.
Associate Professor of Biomedical Engineering

NAWAFLEH, NASHAT MOHAMMAD IBRAHIM

Additive Manufacturing of Short Fiber Reinforced Thermoset Composites (Ph.D., Mechanical Engineering) (May 2020)

Abstract of a dissertation at the University of Miami.

Dissertation supervised by Professor Emrah Celik.
No. of pages in text. (94)

Despite their low cost and design flexibility, additively manufactured, short fiber composites (SFCs) have low strength and stiffness compared to their continuous fiber counterparts. In this study, we overcame this limitation by developing a vibration integrated, auger extrusion system which allowed us the fabrication of SFCs at intricate geometries with high mechanical performance. This thesis treats three main research topics on the principle of using different short chopped fibers. First, short chopped carbon fibers were used as reinforcement which were considered to be too short to enhance mechanical strength of composites with unprecedentedly high strength (>400 MPa), stiffness (53GPa) and fiber volume (46%) up to now. We showed in this study for the first time that, at high fiber volumes of these fibers, a transformation takes place on load transport mechanism within the composites and higher levels of strength and stiffness enhancement were obtained. This fictitious transformation giving rise of short carbon fibers to act as if they are longer, helps effective transfer of tensile loads from matrix to fibers and this results in unprecedented mechanical performance of these material systems. Using these fibers also showed that the mechanical properties of the additively fabricated thermoset composites match those of commonly used structural metals. These properties show nearly isotropic behavior and therefore these composites have great potential to find immediate applications where weight reduction and component complexity are desired.

The second research goal in this work is to fabricate a thermoset-based Kevlar fiber using direct write additive manufacturing. This was also performed by utilizing the developed vibration integrated, auger extrusion system. This system enabled us to apply highly viscous materials based on the presence of Kevlar fibers. We found out that using 6.3% of Kevlar fibers into the epoxy matrix as volume percentage was possible and printed successfully. We also found out that additively manufactured thermoset-based Kevlar fiber with high mechanical performance such as low weight, high strength, and high ductility can be achieved which have a great potential to open doors for wide range of novel applications.

Our third aim was toward the additively manufactured syntactic foams composites. This is due to their advantages over traditionally fabricated foams in terms of design flexibility, in-field fabrication and the low investment cost. Unfortunately, current additive manufacturing methods developed for thermoplastic syntactic foams suffer from unavoidable porosity and low mechanical performance. likewise, in this topic, we overcame these limitations by fabricating thermoset based syntactic foams using direct write additive manufacturing which allowed us to fabricate buoyant syntactic foams with unprecedented strength (>100 MPa) and modulus (1.2 GPa). The achieved mechanical performance of these materials can be tailored by reinforcing the thermoset foams via short carbon fibers. Additively manufactured thermoset based syntactic foams with high scalability and tailored mechanical performance have great potential to find immediate applications where weight reduction, mechanical performance and component complexity are desired.

To my lovely family

ACKNOWLEDGMENT

Firstly, I would like to express my most profound thankfulness to my advisor Dr. Emrah Celik for the endless support of my Ph.D. study and related research, for his perseverance, motivation, tremendous knowledge, and his insightful supervision. I was lucky to have such a great advisor and mentor for my Ph.D. study.

Besides my advisor, I would like to appreciate my thesis committee members: Dr. Ryan Karkkainen, Dr. Edward Dauer, and Dr. James Coakley, for their beautiful encouragement and remarks, which prompted me to extend my research from different outlooks.

My sincere thanks also continue to Eng. Jorge and Eng. Nader, who afforded me such a great opportunity to access Johnson & Johnson laboratory and its research facilities. Without their valuable assistance, this work would not be possible to be conducted. Also, I cannot forget expressing my huge gratitude to my roommate Omar for his continuous support throughout writing this thesis and in my life in general.

Last but not the least, I am forever indebted to my family for providing me great moments and experiences that have made me who I am.

"When one door closes, another opens; but we often look so long and so regretfully upon the closed door that we do not see the one which has opened for us."

-Alexander Graham Bell

TABLE OF CONTENTS

LIST OF FIGURES

LIST OF TABLES

CHAPTER 1: INTRODUCTION

Composites are reshaping the world we live in. In fact, composite materials possess great mechanical performance compared to the traditional engineering materials which allows for significant reduction in weight and cost for certain applications. Composites can be manufactured by traditional fabrication methods or by newer means such as additive manufacturing. Additive manufacturing has advantages over traditionally fabricated composites in different aspects such as design flexibility, saving time, and reducing the investment cost. In the same fashion, additive manufacturing (AM) has paved the road to have a notable change in the generated processes that can help us in producing complex products with specific characteristics in different areas of application varying from aerospace, automotive, to biomedical. Moreover, AM of composites has allowed researchers to develop, change, and expand the properties of generic materials through introducing reinforcements.

This chapter reports a comprehensive view of composites and AM process of these materials. Different AM processes, various material formulations, mechanical performances and drawbacks of these material systems are considered. Emphasis is paid in this chapter on identifying the potential of AM technology for fiber-reinforced composites.

1.1. Composite Materials

Composite materials can be defined as a multi-material system consisting of two or more constituents put together without any chemical reaction. It should be noted that individual materials are used to create a new material which has new features that are not a copy of any of the ingredients taken separately [1, 2].

The components are not soluble in each other, and can be classified into two major phases, namely the reinforcing phase, and the matrix phase. The reinforcing phase is embedded inside the matrix phase, and can be in different forms such as fibers, particles, or flakes [3]. In contrast, the matrix material is in continuous form, as seen in concrete, for example [4].

Detailed examinations reveal the critical roles of the matrix material. The matrix can give the final shape to the composite part, keep the reinforcements in place, and transfer the stress to the reinforcements. In addition to that, it can protect the reinforcing phase from environmental issues such as chemicals, moistures, and degradation [5-7].

Although the matrix phase has an essential contribution to the debate, it commonly suffers from the weakness in mechanical performance [8, 9]. On the other hand, the reinforcing phase material is durable and can be used to strengthen the matrix [10, 11]. Enhancement on strength, stiffness, and fatigue resistance are some of the mechanical properties achieved by using the reinforcing phases as reported in many research papers [12-16]. For example, carbon fibers are utilized as a reinforcing phase to enhance the epoxy resin matrix phase [17].

Composite materials do not only provide remarkable mechanical performance, these materials also possess significant reduction in their weight, better corrosion resistance, and more satisfying durability in different areas of applications such as aerospace, marine, and automotive industries [18-23].

As we have provided insights on the matrix phase being used in composites, there are two major categories of the matrix phase materials—specifically, thermoplastic and thermoset. In general, a thermoplastic, or thermo melting plastic, is a plastic polymer material that softens and melts at elevated temperatures and becomes solid as it cools

down. Thermoplastics may be reshaped because the bonds are weak due to the presence of the van der Waals interactions in these materials. They are typically utilized to fabricate components by different polymer processing methods such as injection molding, compression molding, and extrusion. Typical examples of thermoplastics include polyethylene, polystyrene, polyether–ether–ketone (PEEK), and polyphenylene sulfide (PPS) [24-27].

On the other hand, in thermoset polymer or as know by resin, the molecules are chemically joined together by cross-links. Cross-linking reactions are initiated by the addition of compounds like curing agents, activators, and catalysts [28]. High temperatures can drive the reaction process, and therefore, these polymers cannot be reused once cross-links are formed on curing [29]. Furthermore, thermoset polymers are insoluble and infusible after curing because the chains are rigidly joined with strong covalent bonds. By comparison, they are used with several types of reinforcements, mainly because of the ease of processing due to their low viscosity [30-32].

The main drawbacks of thermoset polymers are their limited storage life at room temperature, their long curing cycle for solidification, and the long fabrication process time [33, 34]. Thermosets possess a well-bonded three-dimensional molecular structure after curing. In addition, instead of being melted as in thermoplastics, thermoset material is decomposed at elevated temperatures. Since these materials can withstand higher temperatures without melting and softening, they are more suited as matrix materials for temperature resistance required advanced conditions in reinforced composites [35]. Typical examples of thermoset include epoxies, polyesters, phenolics, and polyamide [36].

This study will focus on the use of thermoset materials as a base resin (matrix) in composites. As a result of the strong chemical bonds between reinforcements and resin, high mechanical performance can be achieved by the created composite [37-39]. More details on the strength enhancement concept will be explained in the upcoming sections.

1.2. Additive Manufacturing of Fiber-Reinforced Composites

In this section, the most recent academic studies on additively manufactured composites will be reviewed. The desired reinforcements, contents, printing settings to fabricate fiber reinforced composites, mechanical testing methods**,** and the achieved mechanical properties will be outlined.

Additive Manufacturing (AM) or 3D printing is a fast-growing manufacturing technology which allows fabrication of complex freeform geometries via layer by layer deposition. In traditional subtractive manufacturing, different instruments or tools (i.e. milling, drilling, grinding and turning) are used to cut away bulk material to generate the desired 3D structure [40]. In contrast, AM has the ability to fabricate these 3D structures by adding one layer at a time achieving greater complexity with a single instrument in a reduced time and material [41]. As a result, AM has found numerous applications especially in the 3D design and prototyping fields.

The design and manufacturing of lightweight composite materials are attracting growing interest due to their immense potential to replace the traditional engineering materials for structural applications. This interest has accelerated recently due to the reduced weights in additively manufactured components, which can be enhanced with topology optimization without sacrificing the structural performance. Additive manufacturing technology allows for the fabrication of materials in complex geometries. Therefore, components can be redesigned with this freedom of

manufacturability, and the reduction in weight can be further increased if low-density materials are used in additive manufacturing [42-53].

Composites, as described before, are a chosen mixture of different materials with a precise microstructure and shape. This combination leads us to have a unique mechanical performance that are improbable to have with any of the ingredients alone. The characteristics of any composite rely mainly on the properties of its elements, their inside construction, and their volume/mass percentages. Usually, reinforcing material plays a role in determining the strength and stiffness of any composite material [54].

The cooperation between the enhancement material and the matrix is considered to be effective in the cases of the load-bearing system where the matrix cannot be without the interface. The interface works as a tier and transports load between the matrix and the reinforcing fibers. According to that, the mechanical properties of a composite are governed by the interface. Enhanced creep resistance, stiffness, strength, and fatigue represent desirable properties in the composite material systems [55].

Composites can be classified into fibrous composites, particulate composites or nanocomposites according to the size of the reinforcement [56]. The reinforcements in fibrous composites are in the form of fibers in which the length of the fiber is much higher than its cross-sectional dimensions. Besides, the cross-sectional dimensions will be in the order of microns, and length will be in the order of millimeters or centimeters [57, 58].

Further classification of fibrous composites is possible as single layer composites or multi-layer composites depending upon the number of layers. In the same way, fibrous composites can also be classified depending on the length of the fibers as short fiber composites and continuous fiber composites[59, 60].

In short fiber composites, the fibers can be mixed with the resin system, and the composite product can be obtained by compression molding. This provides composites of fibers with random orientation [61-63].

On the other hand, the length of continuous fibers can elongate to the entire size of the component itself. This fiber type is regularly used in high-performance composites. It has been well documented that mechanical properties like strength, modulus, and toughness improve with increasing fiber length [64-68].

Investigations on failure have revealed that under loading, the cracks start at the fiber ends and propagate along with the fiber-matrix interface where these ends are considered as sources of stress concentration. Most high-performance composites are typically strengthened with much longer fibers [69, 70].

Although the manufacturing of fiber-reinforced composites has been reported traditionally by several methods, the additive manufacturing (AM) procedure was mainly implemented to fabricate thermoplastic composites with short fiber reinforcements [71-73]. Additive manufacturing of polymer composites reinforced with continuous fibers, however, has several geometric and processing constraints, including a minimal deposition length and minimal corner radius [74].

Manufacturing with short fibers allows considerably more freedom in the fiber placement and material deposition, which results in more straightforward processing of the material. Material cost and void content are also relatively lower in short fiber composites, which make short fibers an attractive option for many AM applications. Multiple studies exist in literature where chopped polymer , glass [75], and carbon fibers [62, 72] were mixed with thermoplastic resins such as PLA and ABS.

Short fiber reinforced composites were fabricated by melting and extruding a thermoplastic polymer matrix using the fused filament fabrication (FFF) additive manufacturing method. In these studies, significant increase in tensile strength and elastic modulus were observed compared to the neat, unreinforced thermoplastic matrix with the addition of short fibers. Enhanced stiffness in these composites significantly reduced the distortion and warping of the material during processing and allowed for 3D printing of larger-scale components in different applications.

Even though the mechanical performance has been improved in the fused filament fabrication (FFF) method, thermoplastics commonly suffer from drawbacks that are generally seen in the large porosities, the problematic inadequate adhesion within layers, and the multistep process [76, 77].

Overcoming some of the limitations of the FFF of polymer-based material is possible by utilizing the direct writing (DW) additive manufacturing methodology. This method is based on using thermoset materials instead of thermoplastic materials [78]. This is due to the fact that the adhesion between fibers and the polymer matrix in thermoset composites is much higher compared to that of thermoplastic composites [79]. In thermoset composites, it is a common practice to coat the fibers with a thin layer of surfactant (a.k.a sizing) that chemically couples the thermoset matrix and the fiber, creating a strong adhesion. In thermoset composites, the liquid resin can also wet the fiber surface and facilitate the chemical adhesion process [80].

The direct writing system involves preparing highly viscous, printable materials in paste form, which is obtained by modifying the fluid viscosity and yield strength using rheology modifiers, such as nano clay.

Since material melting is not needed for printing, temperature resistant thermosetting polymers with high structural performance are printable with this method without fabricating a precursor filament [81].

Direct write additive manufacturing was introduced by Compton and Lewis [82] to fabricate carbon-fiber-reinforced epoxy composites in 2014 and has been adopted by several research groups to fabricate different thermoset matrices (epoxy [79, 83, 84], cyanate ester [85], bismaleimide [86]) reinforced with short carbon [81, 87] fibers.

Researchers did not focus only on the type of additive fibers. Recent studies [88] also investigated the effects of fibers' alignment on the mechanical properties in AM thermoset composites. They found that 90% and 66% of the theoretical tensile modulus and tensile strength, respectively, have been achieved successfully in composites with a high degree of fiber alignment and low porosity in this study.

1.3. Limitations of Fiber-Reinforced AM Composites

As shown in Figure. 1.1, although thermoplastic composites could be fabricated and 3D-printed successfully with high volumes (~40%) of short fibers, the maximum tensile strength of these composites was still low (<100 MPa). This was due to the porosity between the print lines (unavoidable in the FFF process) and poor interfacial adhesion between the fibers and the thermoplastic matrix. These processing issues limited the strength and therefore applications of additively manufactured thermoplastic composites. On the one hand, thermoset composites provide much higher strength due to the excellent chemical coupling between the fibers and the thermoset matrix and their lower porosity.

Additive manufacturing of these systems, however, is extremely difficult over 5% fiber loading, which is required to achieve high levels of mechanical strength and stiffness.

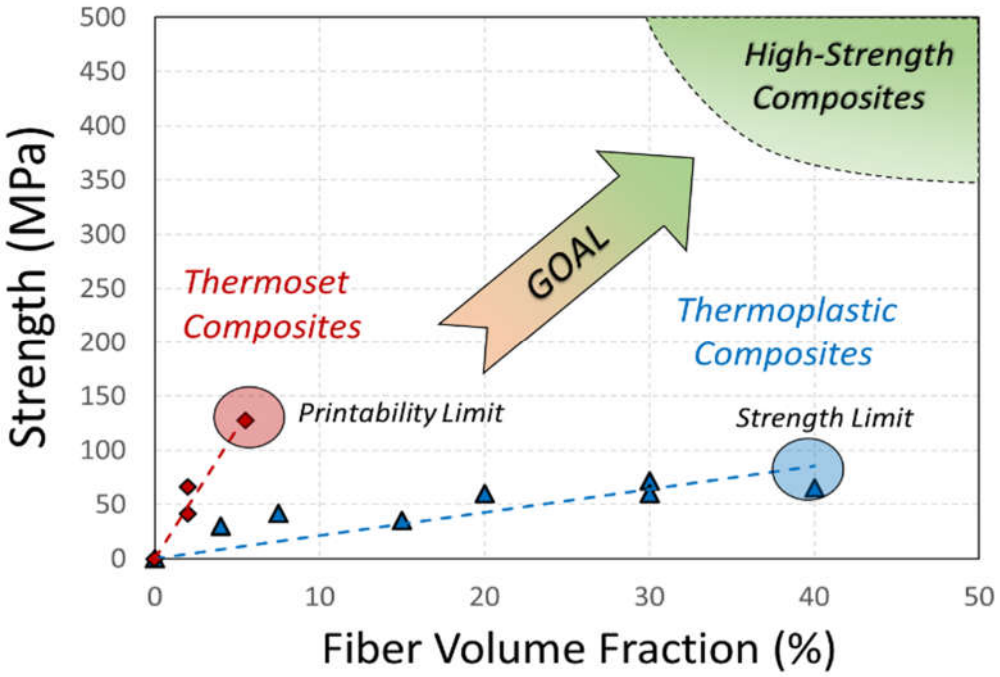

Figure. 1.1: *Strength versus fiber volume fraction charts for the existing studies [71, 72, 81, 82, 89-91] on the short fiber reinforced thermoplastic and thermoset composites.*

Therefore, the main goal of this study was to develop the technology and identify the material systems to additively fabricate short fiber reinforced thermoset composites. Developing the AM technology for high-strength composite materials at low cost will generate a tremendous impact on the adaptation of these materials to wider scales. To achieve this goal, we aimed to overcome the challenges existing in direct-write additive manufacturing of short fiber reinforced thermoset composites, which limit the fiber volume fraction in these systems. In other words, we aimed to enhance the strength of the composite material using the highest possible volume fraction of additive carbon fibers.

In addition, we noticed that some fibers such as Kevlar have a unique combination of low density, high strength, and high ductility compared to other fibers. However, the application of Kevlar fibers during the printable ink preparation in the direct writing process is cumbersome. This is because of the high flexibility of Kevlar fibers which

make them very hard to break during the ink preparation process. As a result, there is a limitation in the number of studies using short Kevlar fibers as reinforcements. However, in this study, we intended to overcome this limitation by fabricating Kevlar fiber reinforced thermoset composite samples using the DW method as our second research goal.

1.4. Additive Manufacturing of Syntactic Foam Composites

Syntactic foam is defined as a composite material system which is prepared by filling polymer, metal, or ceramic matrix with pre-formed hollow spheres [92-94]. Due to the closed-form and lightweight of the hollow sphere constituents, these foams possess low density and high specific strength properties. As a result, these materials find a range of applications where low water absorbency, buoyancy, resistance to the long-term hydrostatic pressure, and a high impact endurance are demanded [95, 96].

Glass microspheres (also known as micro balloons or glass bubbles) are the most common constituents in syntactic foams. Glass microspheres have a diameter range of 10 to 300 μm, and they are utilized in syntactic foams due to their higher compressive strength compared to other microsphere types.

Syntactic foams filled with glass microspheres have been fabricated with conventional manufacturing methods such as injection and compression molding, and their mechanical properties have been investigated [97-103]. To fabricate syntactic foam components at complex geometries without tooling, additive manufacturing possesses great potential.

In addition to the unmatched design freedom, AM also offers low investment cost and fast design-to application process benefits as well. AM of polymer matrix syntactic foams was introduced recently using a fused filament fabrication (FFF) method [104,

105]. In these studies, glass microspheres-filled precursor filament was initially prepared, and this filament was used to fabricate syntactic foam parts in a layer by layer fashion.

These studies showed the feasibility of AM of polymer matrix syntactic foams. However, high porosity, low strength, weak adhesion between the layers and the multistep fabrication process are the drawbacks of the FFF based manufacturing of syntactic foams [75, 106]. In this research, our third goal was to investigate AM of thermoset-matrix syntactic foams using the direct-write methodology for the first time with the goal of fabricating these syntactic foams with high strength and temperature resistivity, which cannot be achieved via thermoplastic matrices. In addition, this study explores the tailorable mechanical properties of syntactic foams via addition of short carbon fibers. Therefore, a novel methodology for the preparation of thermoset-matrix syntactic foams and syntactic foam composites via DW manufacturing is reported in this study, and the mechanical performance of these materials is compared against the previously reported studies.

1.5. The Structure of This Dissertation

This thesis research focuses on additive manufacturing of thermoset-based polymer matrix composites and understanding the effects of different types of fiber reinforcements on the mechanical performance of the additively manufactured composites. The composite materials consist of epoxy matrix and discontinuous fibers used as reinforcements. The fibers types investigated in this study are Carbon and Kevlar. As the last step in this thesis, additive manufacturing of ultra-lightweight composites using syntactic foam materials will be introduced. In addition, carbon fibers will be mixed with foam material to tailor the mechanical performance. Evaluation of

these fibers and the criteria behind choosing them will be separately discussed in the next chapters. The construction of this dissertation is divided into six chapters according to the following arrangement:

• **Chapter 1: (Introduction) -** Concise explanation of the concepts of the composite materials, including a review of the case of the art in composite additive manufacturing, specifically in fiber-reinforced thermoset composite, challenges, and aims followed throughout this project is provided.

• **Chapter 2: (Materials and Methods) –** In this part, materials and tools used in fabricating the test specimens are presented. Also, methods used during the 3D printing process are mentioned. Furthermore, a review and investigation of three different mechanical test types will be explained precisely.

• **Chapter 3: (Additive Manufacturing of Short Carbon Fibers Thermoset Composites) –** The first major goal of this thesis is discussed in detail in this chapter. First, this chapter will examine the effects of the addition of chopped carbon fiber into neat epoxy on specific mechanical properties of printed structures. Second, the effects of adding different amounts of carbon fibers on the printing ink are presented via the rheology measurements. Third, the performed mechanical tests are examined to quantify the reinforcing ability of these fibers within the fabricated composite material. Finally, hierarchical microstructures of the composites will be explored using scanning electron microscopy.

The fracture surfaces will be investigated after performing the mechanical tests to investigate the defects and artefacts such as porosity, infill, and material interdiffusion, which are inherent drawbacks of the 3D printing process.

• **Chapter 4: (Additive Manufacturing of Ductile Kevlar Fibers Thermoset Composites)** – The second type from the chopped fibers is explained in this segment. First, we will discuss the properties of Kevlar fibers. Second, since there are no commercial chopped Kevlar fibers, the method used to produce short Kevlar fibers from continuous commercial fibers will be presented. Third, in the same fashion, this chapter will shed light on the addition of chopped Kevlar fibers and their effects on mechanical performance. The amount of fibers that are added, their rheology, printing process, and the hierarchical microstructural will be described.

Finally, mechanical tests included in the previous chapter are presented here again. However, an investigation of the fatigue mechanical test, which is used for the first time in AM of Kevlar fiber reinforced thermoset composite, will be shown in this chapter.

• **Chapter 5 (Additive Manufacturing of Syntactic Foam Lightweight Thermoset Composites) –** This chapter will mainly concentrate on the fabrication of lightweight materials. Glass microspheres this time are used to produce lightweight composites. However, for the first time, we could apply this material in AM thermoset printing to create specimens. Although we could generate lightweight samples; the mechanical performance was not sufficiently strong. To solve this issue, the addition of short carbon fibers to the glass microspheres is provided and explained to enhance some of the mechanical properties. Both flexural and compression tests are performed to investigate the mechanical properties. Also, the hierarchical microstructural will be presented.

• **Chapter 6: (Conclusion and Future Work) –** In this final chapter, the conclusions of this work are manifested as well as proposals for the future work and the continuation of the research.

CHAPTER 2: MATERIALS AND METHODS

This chapter will include a concise overview of the 3D printing process methods, including the interest of using Direct Write (DW) additive manufacturing technologies compared to the Fused Filament Fabrication (FFF). The core components of the printed materials used in this study to overcome the current limitations in this field of research will be explained in detail.

2.1. Comparison of FFF and DW Additive Manufacturing

FFF is one of the most well-known additive manufacturing methods for creating 3D polymer parts. Thermoplastic polymers such as Polylactic Acid (PLA), Acrylonitrile Butadiene Styrene (ABS), are commonly utilized in this method. These materials are used in filament form which is inserted toward a heating element via a Bowden tube. Extrusion can be performed by heating the filament to just above the melting temperature. Therefore, the material will be liquid after melted and can be deposited in small strips on the print bed, as shown in Figure. 2.1 below.

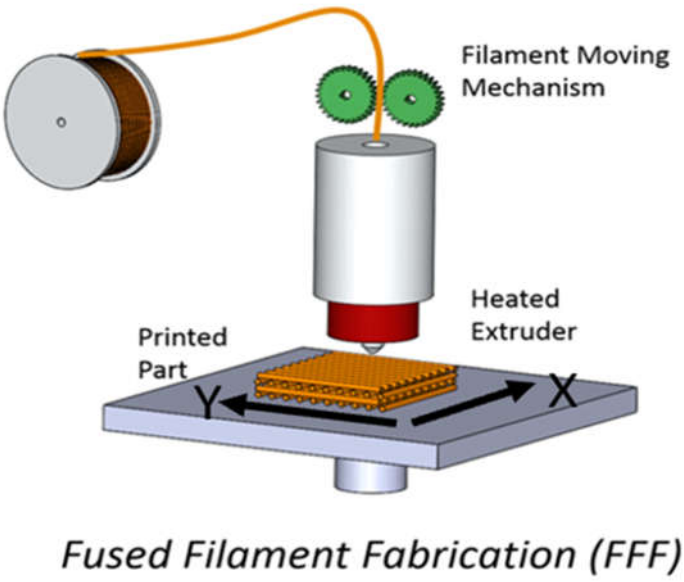

Figure. 2.1: *Schematic overview of how the material is deposited in FFF processes.*

The principle of the FFF 3D printing process is based on the movement of the print bed or print head (or the nozzle) in the x-, y-, and z- directions. The primary function of the print head is to deposit the layers of material. Once the first layer is formed, the print bed/head will shift downward/ upwards, and a next layer can be deposited over the first one until finishing the desired part. Typically, to ensure that the initial print layer has sufficient adhesion to the print bed surface, the printing surface can be treated with a glue or other adhesive substances before starting the fabrication process.

The advantages of the FFF method can be noted in different aspects. First, an extensive diversity of materials is possible to use. Besides, these materials are easy to handle and change during the printing process. Second, it has high resolution can fabricate samples in a short period of time. Third, to enhance mechanical performance, reinforcements such as particles, fibers can also be added into the thermoplastic matrix. Finally, the low cost and the easy maintenance make it one of the best choices for researchers in various fields of applications.

Despite these advantages, however, there are some deficits to this method. These drawbacks are the low service temperature in thermoplastics and the voids between the deposited strips during the printing process. In addition to the porosity, poor interfacial adhesion between the reinforcements and the thermoplastic matrix limits the mechanical performance and, therefore, the applications for this technology.

The process known as direct writing (DW) has significant advantages to eliminate some of the drawbacks of thermoplastic printing described above. DW is similar to the FFF method in terms of creating objects. The deposition of layers upon layers on the printed surface can generate the final part. However, instead of the FFF process, which is based on polymer melting and solidification, the direct-write technique is used for the additive

manufacturing of liquid thermoset materials. Viscous pastes are prepared by mixing liquid polymer resins with fiber reinforcements and rheology modifying nanoparticles. These pastes have sufficient yield strength to be extruded into intended geometries. Additionally, since material melting is not required for 3D printing, temperature-resistant thermosetting polymers are printable with this method. As the last step of the manufacturing process, the extruded material is cured via heat or light into solid structures. Figure. 2.2 illustrates this method.

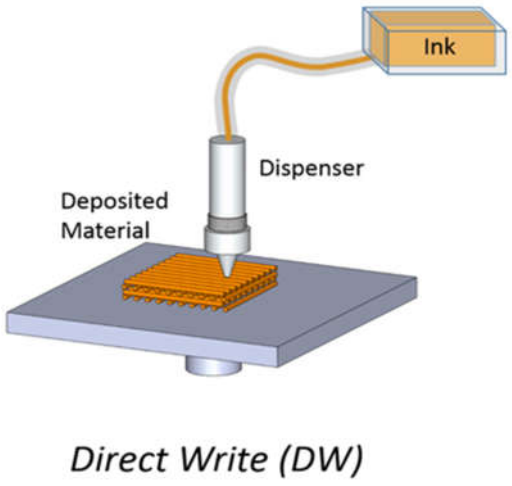

Figure. 2.2: *Schematic overview of the DW processes.*

It is found that the adhesion between reinforcements and the polymer matrix is much higher in thermoset composites compared to thermoplastics, where these reinforcements can be coated with a thin layer of surfactant which chemically couples the thermoset matrix creating a strong adhesion. For example, in thermoset composites, the liquid resin can wet the fiber surface and facilitate the chemical adhesion process. It should, nevertheless, be borne in mind that the main parameters of printing in DW method must be optimized to build up the required parts with high mechanical performance.

It is certainly true that there are lots of parameters which can be applied, but there are some parameters being considered as the core of this printing process. These main parameters include the print head velocity, layer height and width, and the viscosity of the ink.

In this respect, it is found that when the print head velocity is too high, the deposition of material will become discontinuous, resulting in weaker mechanical features and lower overall quality. On contrast, when the velocity is too low, the deposited ink material might overflow resulting in more poor mechanical properties. Researchers also verified that minimizing the layer height in the z-direction can sharply increase the printing resolution. In other words, the thinner the layers are, the higher the dimensional precision of the part is. Therefore, the minimum layer thickness possible will generate the most accurate parts. Lastly, the viscosity of the ink, which is determined by the amount of additive reinforcement material, controls the process.

The physical properties of the prepared ink are important parameters during the printing process. Inks with too low viscosity can be printable but the printed ink does not retain shapes. On the other hand, printing highly viscous ink material requires high extrusion pressures and can be very challenging. Therefore, viscosity should be maintained in a certain range to perform the printing process. The following section will set out the required tools, methods, and instruments which are used to fabricate the fabricate test specimens.

2.2. Direct Write Printing Process Tools

2.2.1 Geometry Design and Slicing Software

The specimens for mechanical testing are determined according to ASTM standards (Standard Test Method for Flexural Properties of Polymer Matrix Composite Materials). These samples were designed using Creo Parametric V5 2019 computer aided design (CAD) software, and the ASTM standards were used to determine the critical dimensions of the specimens.

CURA software was chosen to be the main slicing program in this thesis, where it can serve as the interface linking the computer model and the printer. To understand the working principal of CURA program, the part geometry that is created in Creo can be transported as an STL file and imported into CURA.

In other words, this is the main connection between this software and the design program. The STL file can also be transformed into G-Code through CURA. 3D printers can understand the G-Code language created to perform the required tasks. CURA software is has user-friendly graphical user interface and has numerous choices for altering, or sometimes remodeling the STL-files, according to the users' coveted stipulations to tailor the part and attain the aspired properties for the application.

2.2.2. ***Delta Bot Hackka V1 3D Printer***

A commercial FFF type of 3D printers was used in this research, namely, Delta Bot Hackka V1 and Figure. 2.3 represents the actual image of this printer.

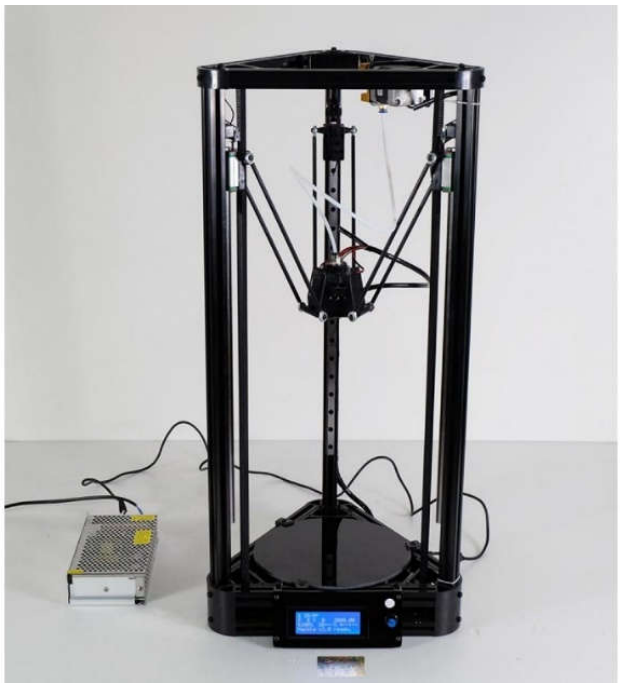

Figure. 2.3: *Delta bot 3D printer[107]*

Although it has a small size which is about 300 mm in width and 680mm in height compared to other 3D printer families, this printer can surpass or emulates other 3D printers in their functionality and can do the same required missions. The greatest benefit of this printer is its high speed, and high resolution that can reach up to 100mm/s, and 0.005 mm respectively.

In conjunction with this, this printer is compatible with many slicing softwares such as CURA, Slic3er, and others. Also, different material types such as ABS, PLA, Nylon, and others can be used in this 3D printer.

FFF printers are specifically designed for fabricating thermoplastic materials. On the contrary, this research focuses on the DW method, which concerns with

thermoset materials. Initial questions we asked ourselves were the following: How could we modify this printer to fabricate thermosetting polymers in our study? And what are the following steps that have been used to make that is possible? Answers for these questions are specifically presented in the following sub-section to describe the modification process.

2.2.3. ***The Customized 3D Printing Setup***

The few commercially available 3D printers that are designed to print thermoset materials. However, these printers are either expensive or designed for additive manufacturing of thermosets rather than thermoset composites. Therefore, a custom-made 3D printing setup was designed in this study.

In a standard FFF printer, thermoplastic filaments are pushed through a gearbox into the extrusion nozzle. Besides, the printer head is specifically designed to melt the solid material at high temperatures. Since the thermoset materials need no melting, the printhead needed replacement. Figure. 2.4 shows our customized system which will be described it in the next paragraphs in details.

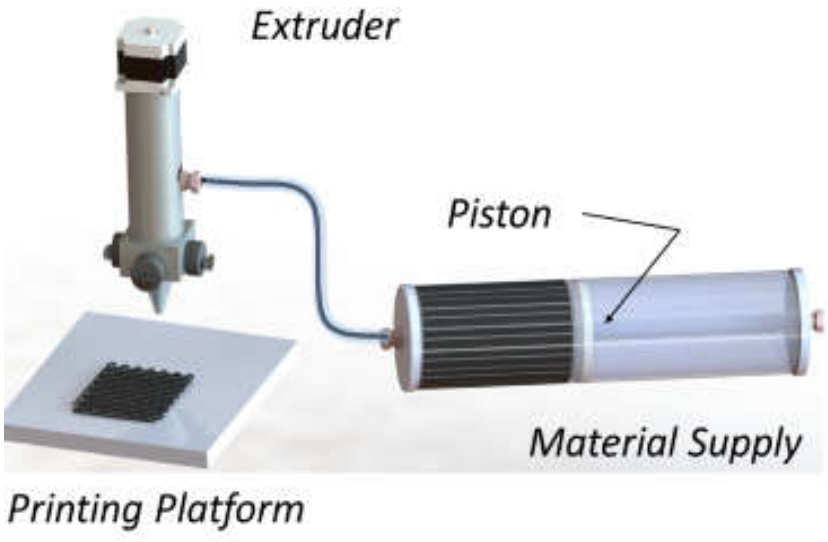

Figure. 2.4: *The Customized 3D printer Kit*

This 3D printing system is designed for the deposition of viscous materials such as fiber reinforced composites. In addition, it supports printing at high speeds and can be used with various nozzle diameter sizes from 0.1 mm to 3 mm. The 3D printing system has two major components. The first part is the material container. In this material supply system, viscous ink is pushed toward the extruder via a piston driven by a stepper motor. Since the diameter in this container is large, the amount of pressure needed to push the material is minimum, and consequently, high viscous inks are pushed toward the extruder successfully.

The second part of the system is the extruder or material dispenser. In general, the main function of the extruder is to dispense the material on the surface for 3D printing. The weight of this part is small, and it is noted by its flexibility to be placed in four various adjustments to outfit any printer. Highly viscous materials can be extruded as a result of using a strong stepper motor connected to the extruder as shown in Figure. 2.5.

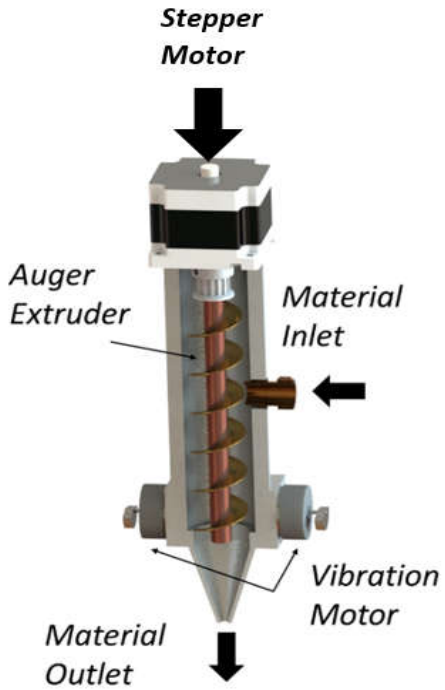

Figure. 2.5: *Extruder cross sectional view for the Direct Write system.*

As the stepper motor shaft rotates, the auger screw inside the extruder will rotate and push the material downwards during the printing process. The rotation speed of this motor was controlled and optimized through a control unit that is compatible with most of the FFF 3D printers' motherboards. In other words, the stepper motor speed can be modified by adjusting the micro-steps/mm inside the G-code using the command *M92 Exx,* where *xx* represents any integer number. This number literally indicates the number of micro-steps number per mm.

The rotation speed will increase by increasing the micro-steps numbers, and as a result, the amount of the material that comes through the nozzle will increase. This extruder is also equipped with multiple vibration motors, which simultaneously shake the nozzle and extruder channel walls, avoiding material adhesion and fiber agglomeration. The use of these motors significantly reduced nozzle clogging and provided consistent material flow at high fiber loadings.

2.2.4. ***Thinky AR-310 Shear Mixer***

It is challenging to separate, or mix, viscous inks using conventional mixers. For this purpose, a high-shear mixer should be used to mix homogeneously viscous materials (i.e., thermoset resins). In order to mix at high shear, several factors should be considered in choosing a suitable mixer which can fit the purposes. Examples for that are the diameter of the rotor, rotor speed, mixing time, and the distance between the stator and the rotor. Based on what we explained above, and after investigations, we decided to use Thinky AR-310 high-shear mixer as shown in Figure. 2.6. This mixer is able to mix wide range of materials which are up to 350 grams in weight such as ink, epoxy resin, solder paste, etc. Its high safety, lightweight, novel tilting design, steady performance, easy operational, and easy maintenance address this mixer as the first choice in our research.

Figure. 2.6: *Thinky AR-310 shear mixer [108]*

2.3. Ink Preparation

The composite inks were prepared by mixing the epoxy resin (EPON Resin 826 from Hexion), curing agent (hardener) from Sigma-Aldrich (1-Ethyl-3-methylimidazolium dicyanamide), and Garamite-7305 nanoclay from BYK additives as a rheology modifier.

Afterwards, chopped fibers were then added gradually to this mixture in different amounts to observe their effects on the mechanical properties and printability. The volume percent of these fibers within the composite varied from 2% up to 46% according to each fiber type. On the other hand, as the presence of fiber content increases in the composite ink mixture, the amount of nanoclay will gradually be reduced to keep the viscosity at a similar level since. The nanoclay content corresponding to the fiber amounts will also be explained in the next chapters.

The inks were subsequently shear mixed using a high shear mixer (Thinky ARE-310) for 3 minutes at a speed of 2000 rpm to ensure homogeneity. After mixing the fibers, epoxy matrix, and the clay rheology modifier, latent curing agent (hardener) from Sigma-Aldrich (1- Ethyl-3-methylimidazolium dicyanamide) was added and mixed for 1000 rpm for 1 minute as the last step of the ink preparation.

2.4. General 3D Printing Process in This Research

As a first step in this research, we decided to fabricate samples based on the fact of mixing only rheological nano clay powder to adjust the viscosity of the epoxy in the ink preparation process. After adding 10% from the nanoclay as a weight percentage from the resin, the mixtures then were subsequently shear mixed using (AR-310) mixer for 3 minutes with a speed of 2000 rpm to ensure homogeneity as described in the previous section.

In this step, the ink is ready to be deposited throughout the 3D printer used in this research (i.e., Delta bot 3D printer). However, prior to the printing process, rectangular prism-shaped test specimens, in accordance with ASTM D7264/D7264M− 07 standard, were designed in Creo Parametric V5. The specimens have a simple geometry, and the customized 3D printing setup was used to deposit the ink through a 0.60 mm nozzle diameter using the 3D printer in the longitudinal direction (0^0) as shown in Figure. 2.7.

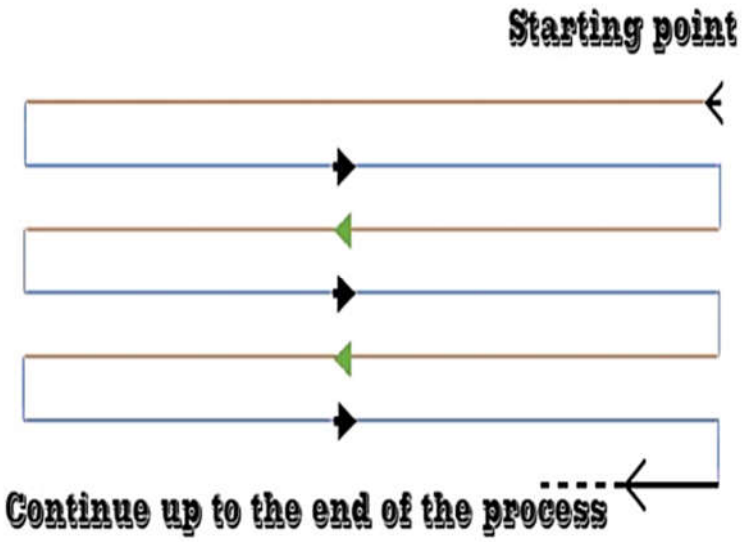

Figure. 2.7: *Nozzle path of a single layer during 3D printing*

The printing speed was maintained at 40 mm/s, and throughout the printing process, the temperature of both build plate and nozzle were kept at room temperature. The build plate was covered with a 20 µm thickness Teflon sheet for easy removal of the parts after the curing process, which was carried out in an oven under a temperature of 100^0 C for 15 hours. The resulted samples are shown in Figure. 2.8.

Figure. 2.8: *3D printed base ink samples*

2.5. Mechanical Test Setup

A digital caliper was used in order to determine the width, length, and thickness of the printed samples. The dimensions were checked to be inside the proper tolerances commanded by the ASTM D7264/D7264M− 07 and/or ISO 604 standards for all printed specimens. The results of the measured samples showed that the accuracy of the printed parts was in the agreement with the designed specimens. Three different mechanical tests were performed; flexural, compression, and fracture toughness. All of these testes were accomplished using the INSTRON universal testing machine [109] with a 100 KN load cell.

2.5.1. ***Flexural Test***

Because of the simplicity of three-point bending conditions, this research will focus on a three-point flexural test, according to ASTM D7264/D7264M− 07 standard. Generally, in this test, the span length can be determined according to unrestricted support span-to thickness ratios of 16:1, 20:1, 40:1, and 60:1 that can be applied. In other words, span length relies on the thickness of the sample. In our experiments, 16:1 span-thickness ratio was chosen as a reference to fulfill requisites of the test. Span length is also considered to calculate the specimen's length, where it is normally about 20 % longer than the span length. Flexural strains ε and stresses σ are computed according to ASTM D7264/D7264M− 07 standard test as the following two equations:

$$\varepsilon = \frac{6\delta h}{L^2} \tag{2.1}$$

$$\sigma = \frac{3PL}{2bh^2} \tag{2.2}$$

where δ is the displacement, h is the beam thickness, and L is the support span in Eq. (2.1). P is the loaded force, b and h are the width and the thickness of the beam respectively in Eq. (2.2).

Failed samples were optically analyzed and if the failure did not occur at the center, bending moment arm ($L/2$) in Eq. (2.2) was updated. The flexural modulus was calculated based on the slope value in the strain-stress graph.

2.5.2. ***Compression Test***

Likewise, this test is also adopted to measure some fundamental parameters such as the compressive strength and Young's modulus. The test was performed using the universal Instron machine in the accordance with ISO 604 standard.

The behavior of the materials subjected to a compressive force exhibit a linear relationship between stress and strain which can be translated according to Hooke's Law in the following equation:

$$\sigma = E\varepsilon \tag{2.3}$$

Where E represents Young's Modulus value for under compression, and this value explains the material's deformation under the effective compressive loading prior to the plastic deformation. To expand this point more, once a certain force threshold has been reached, plastic deformation will befall where linear behavior stops. At this point (i.e., proportional limit), the measuring force is known as the yield point of the material. The maximum achievable force at that point will provide the ultimate compressive strength value.

2.5.3. ***Fracture Toughness Test***

Fracture toughness is interpreted as an important phrase for measuring the material's ability to resist the crack's extension especially when using composites in unidirectional fibers. In other words, the more the material resists the crack, the higher the toughness obtained. In this type of test, the direction of the applied load relative to the crack-defect plane determines the type of three modes of loading that can be used in the fracture mechanism. If the load is perpendicular to the crack plane, this is called Mode I. Conversely, Mode II can occur by applying parallel load (in plane-shear) to the crack plane. On the one hand, in Mode III crack is loaded out of its plane. Figure. 2.9 illustrates the three modes.

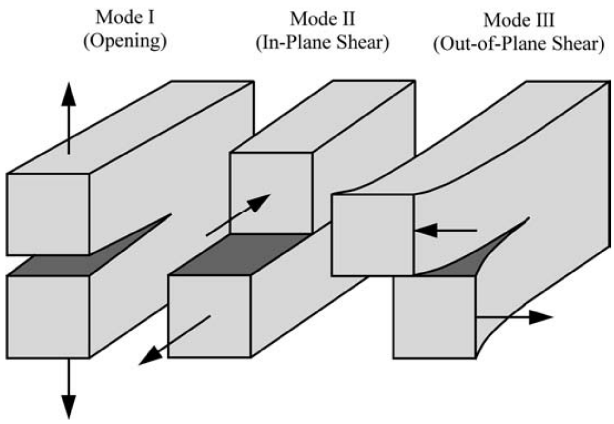

Figure. 2.9: *Modes of loading on the crack surface [110]*

In this thesis, analysis of the generated fracture toughness samples was based on the Mode I, according to the ASTM D5528-01 test. The reason behind choosing this Mode is due to the geometry restrictions. To illustrate more, other modes require samples with a large thickness. However, it is difficult to create samples with higher thickness using thermoset materials because of the lack of immediate solidification that thermoset materials have. Furthermore, after a certain height during the 3D printing, the structure will collapse, and the thickness will not be sufficient to be considered in the standards. In contrast, layer thickness in Mode I is reasonable and ranges from (3-5mm). The constructed samples in Mode I have an initial crack length of 50 mm, and the most common width and length were 25mm and 125mm, respectively. A standard compact labeled part is shown in Figure. 2.10.

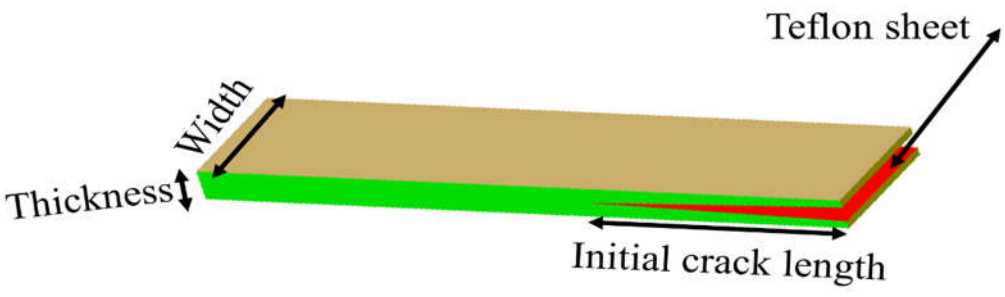

Figure. 2.10: *Actual representative image of fracture toughness Mode I*

It is clearly shown from Figure 2.10 that test specimens are fatigue pre-cracked before doing the test. Pre-cracking produces a sharp crack tip by adding the Teflon sheet in the middle plane of the printed layers to serve as a delamination initiator.

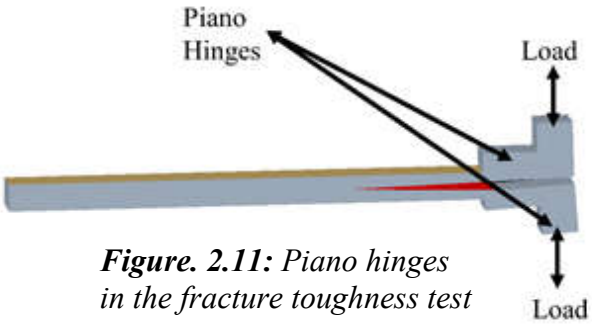

Figure. 2.11: *Piano hinges in the fracture toughness test*

During the test, vertical crack opening loads are applied to the sample by means of the hinges (Figure. 2.11) at the end of the specimen. At each different load, displacement, and crack propagation length are recorded until the maximum load that can break the sample. Afterward, the amount of energy released according to the ASTM D5528 - 01 standard used in this test is calculated according to Eq. 2.4 to quantify the toughness degree of this material.

$$G_I = \frac{3P\delta}{2wt} \tag{2.4}$$

Where G_I is the released strain energy, and P, δ, w, t are the applied load, crack propagation length, width, thickness, respectively.

CHAPTER 3: ADDITIVE MANUFACTURING OF SHORT CARBON FIBERS THERMOSET COMPOSITES

Additively manufactured, short fiber reinforced polymer composites have advantages over traditional continuous fiber composites, that include low cost and design flexibility. However, these composites suffer from low strength and stiffness as compared to their continuous fiber counterparts due to the limitation of low fiber volume. In this chapter, this limitation was overcome for the first time by developing a method that allowed fabrication of short fiber reinforced thermoset composites in intricate geometries, with unprecedented mechanical performance, and high fiber volume ratio.

3.1. Carbon Fibers Used in This Research

Milled carbon fibers with low aspect ratios were used in this study to facilitate continuous extrusion at high fiber loadings. Existing studies [84, 90] on additive manufacturing of short fiber reinforced thermosets utilized relatively long fibers with high aspect ratios in the range of s = 46-234. This selection was consistent with the fact that mechanical loads can be more effectively transferred via long fibers with high aspect ratios and hence higher strengths can be achieved. Using high aspect ratio fibers during material extrusion however leads to the fiber agglomeration, nozzle clogging and printing defects at high fiber loadings. Therefore, in our study, we used milled carbon fibers instead with very low lengths and aspect ratios (L=50 μm, S=4.5). Two types of carbon fibers were purchased from Mitsubishi Chemical Carbon Fiber and Composites (MCCFC); sized fibers (K6371M) and unsized (K223HM) fibers to assess the effect of sizing and the fiber-matrix adhesion on mechanical properties.

Milled carbon fibers (50 microns in length) were added gradually to this mixture in different amounts to observe their effects on the mechanical properties and printability. The volume percent of these fibers within the composite varied from 2% up to 46%. As the carbon fiber content was increased in the composite ink mixture, the amount of nanoclay was gradually reduced to keep the viscosity at a similar level since the carbon fiber addition also increased the viscosity of the ink. The nanoclay content corresponding to the carbon fiber amounts of 0% (base ink), 2%, 5%, 13%, 21%, 28%, 36%, 46% were obtained as 10%, 9%, 8%, 4.5%, 3.6%, 3.3%, 1.9% and 1%, respectively. The inks were subsequently shear mixed using high shear mixer (Thinky ARE-310) for 3 minutes at a speed of 2000 rpm to ensure homogeneity.

3.2. 3D Printing Using Vibration Integrated Direct Ink 3D-Printing Setup

Achieving higher fiber loading over 5% by volume in the previous studies was not possible since the viscosity of the composite ink increased significantly over this fiber volume and therefore extremely high pressures were required to pump these viscous inks through sub millimeter nozzle orifices. Extrusion process becomes even more difficult as the fiber aspect ratio is increased which leads to fiber agglomeration and nozzle clogging.

To extrude highly viscous composite materials, a custom-made direct write extrusion setup was developed as mentioned in chapter two previously (Figure. 2.5). The composite ink is filled into a barrel container with a 50 mm inner diameter and transferred toward the extruder inlet port with a piston driven by a stepper motor. An auger is then used to push this material through the nozzle. This displacement-controlled, 2 step- printing system allowed us to extrude highly viscous composite inks reinforced with high levels of fiber loading. In addition, the extruder is equipped with multiple vibration motors, which simultaneously shake the nozzle and extruder channel

walls, avoiding material adhesion and fiber agglomeration. The use of these motors significantly reduced nozzle clogging and provided consistent material flow at high fiber loadings (Figure 2.6).

Figure. 3.1 shows the effect of vibration on the consistency of flow and the porosity of the printed test samples. The prepared composite inks were dispensed through the tapered nozzles attached to a customized delta 3D printer where the printing speed was maintained at 40 mm/s.

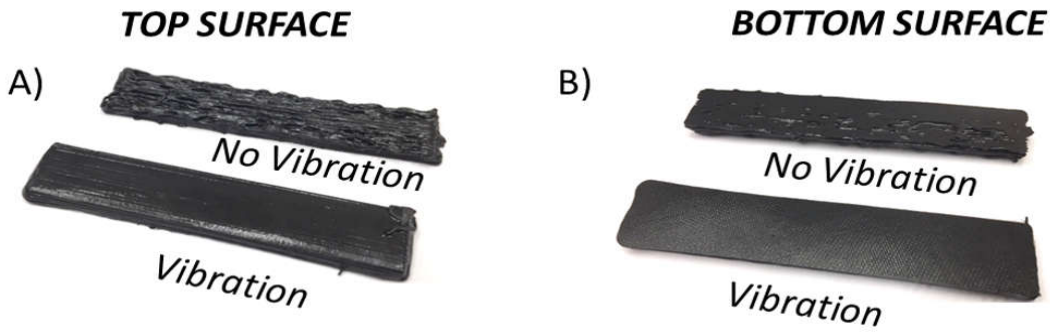

Figure. 3.1: *The effect of vibration on the quality of the composites reinforced with 36% carbon fibers by volume A) Top surface, B) Bottom surface.*

Utilizing milled fibers as the reinforcement along with the displacement-controlled extrusion system described above and integrating a vibration activated nozzle unclogging system allowed us to significantly increase the fiber volume fraction in the thermoset composites.

We could successfully fabricate specimens up to 46% fiber volume fraction with consistent material flow. The material deposition was performed at high geometrical resolution using 0.6 mm tapered nozzles except the highest carbon fiber loading (46%) where slightly larger (0.84 mm) nozzle was preferred to keep the continuity of the material flow.

The curing process was performed at 100^{o}C over the course of 15 hours. Performing post-curing on the printed inks at 200^{o}C for 2 hours did not result any change in mechanical properties or morphology of the composites and therefore, was evidencing that curing at 100^{o}C for 15h was sufficient to achieve 100% curing of the thermoset material.

Fiber content in the fabricated parts was determined using the mass fractions and the densities of each constituent. Mass fractions (parts per hundred) are all known during ink preparation process relative to the epoxy mass. Densities of epoxy, nanoclay, carbon fiber and curing agents are 1.16 g/cc^3, 1.98 g/cc^3, 2.2 g/cc^3 and 1.06 g/cc^3, respectively. Using these density values and the mass fractions, the volume fraction of each constituent and the total density of the fabricated composite specimens were calculated.

3.3. Mechanical Characterization

To assess the mechanical performance of the printed specimens, 3-point bending tests were performed using Instron universal testing machine in accordance with ASTM D7264/D7264M− 07 standard (Standard Test Method for Flexural Properties of Polymer Matrix Composite Materials). At least four tests were performed for each set to provide the repeatability and quantify experimental variability. In addition, a 16:1 span-to- thickness ratio was utilized where the span length was adjusted for each sample to keep this ratio. In addition to printing in the longitudinal direction (print lines parallel to the bending loads), transverse specimens (print lines perpendicular to the bending loads) were fabricated in order to quantify the level of anisotropy in the additively manufactured specimens. Three different fiber volume ratios were selected for the transverse printing: low (5%), medium (20.2%), and high (36.1%). Compression tests were also performed on the composites loaded with the maximum (46%) carbon fiber amount to test to prove that compressive strength is significantly higher than the tensile

strength and therefore, failure occurs only under tension during the 3-point bending tests. ISO 604 standard (Plastics- Determination of compressive properties) was followed in these tests which requires sample size of 10x10x4 mm for strength measurements.

Fracture surfaces of the mechanical tested specimens were imaged using JOEL JSM-6010 PLUS/LA Analytical Scanning Electron Microscope) (SEM). Prior to imaging in SEM, samples were sputter coated with a thin (1-2 *nm*) layer of gold layer under 50 torr for 30 seconds.

3.4. Results and Discussion

Viscosity measurements on the printing inks are given in Figure 3.2. This figure indicates that the neat epoxy showed the minimum viscosity having the range of 15-41 Pa. s throughout the entire shear rate spectrum. Addition of the curing agent slightly increased the viscosity of the epoxy, however, the nanoclay was found to be the major rheology modifier enhancing the viscosity more than 3 orders of magnitude as shown in this figure. Reduction of the nanoclay content as more carbon fiber was added into the printing ink reduced the viscosity which further emphasized the effect of nanoclay as the rheology enhancer on these inks. All inks showed different levels of shear thinning behavior. Shear thinning was minimal in the neat epoxy ink and maximum in all the of printing inks where nanoclay was added solely (base ink) or jointly with carbon fiber into epoxy.

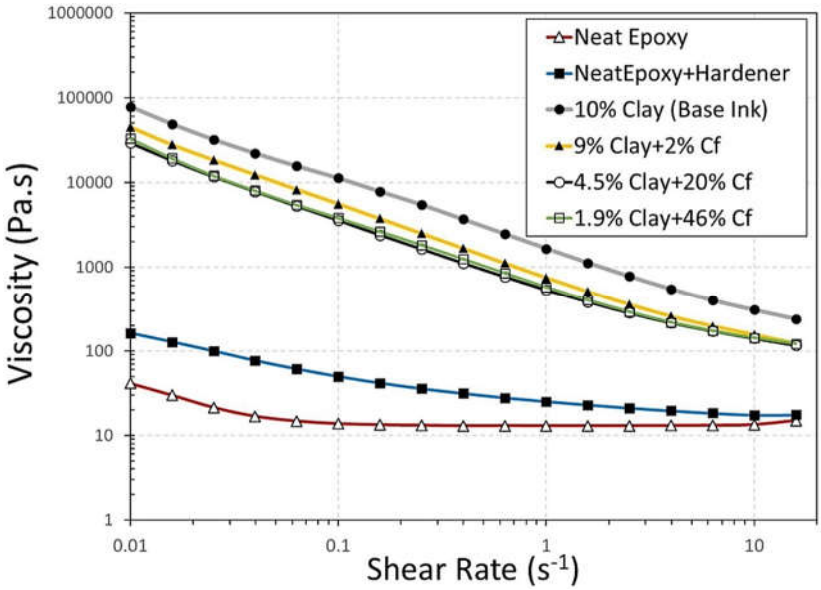

Figure. 3.2: *Variation of complex viscosity as a function of shear rate for the various inks*

Figure 3.3 shows the complex geometries printed using direct ink writing methodology, which denotes the high dimensional accuracy of this technique. The ability of our printing system to fabricate intricate geometries was intact even at the high fiber loadings as evidenced by the similarity of the samples printed with low (2%) and high fiber (46%) loading levels in Figure. 3.3 inset images.

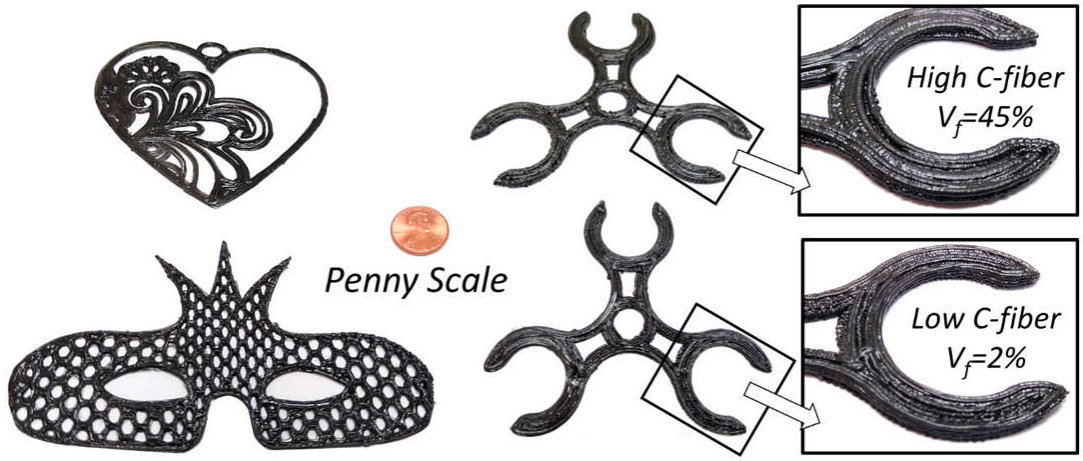

Figure. 3.3: *Images of the complex geometries printed with short fiber reinforced thermoset composites. Figures on the right compares the same 3D model printed with 2% (bottom) and 45% (top) fiber loading. Inlet images are the close-up view images to show the print quality in detail.*

Flexure strength and flexure modulus of the composites as a function of fiber loading are given in Figure. 3.4, where composite strength and modulus increase quite linearly as the carbon fiber amount is increased. To compare the mechanical performance of the fabricated composites to the state-of- the-art published results, flexure strength and modulus properties of 3D printed composites reported by Pierson et al.[84] are marked in Figure. 3.4. As the figure indicates, a nearly 3-fold increase in strength and 5-fold increase in modulus were observed as compared to this recent study where the maximum strength and modulus were reported up to date for short fiber reinforced composites.

The dramatic increase in strength and modulus in our study was mainly due to our ability to increase the fiber volume level from 5% to 46% using the extrusion system described above. The figure also shows that for the same amount of fiber loading (~5%), a slightly lowered mechanical performance was achieved using milled fibers (S=4.5) compared to those reported for significantly higher aspect ratios (S=63) reported by Pierson et al. This comparison shows the great potential of milled fibers for the fabrication of high strength composite materials and will be discussed further in the upcoming paragraphs.

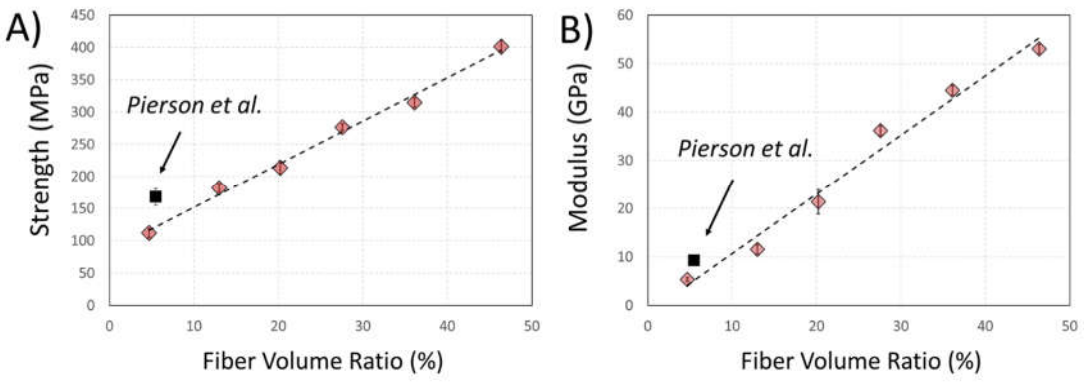

Figure. 3.4: *Flexure strength versus flexure modulus variation of additively manufactured carbon-fiber reinforced composites as a function of fiber loading levels.*

Fracture surfaces of the composite specimens were imaged using a scanning electron microscope (SEM) following the mechanical testing. Figure. 3.5 represents SEM pictures of the specimen reinforced with 46% carbon fibers by volume.

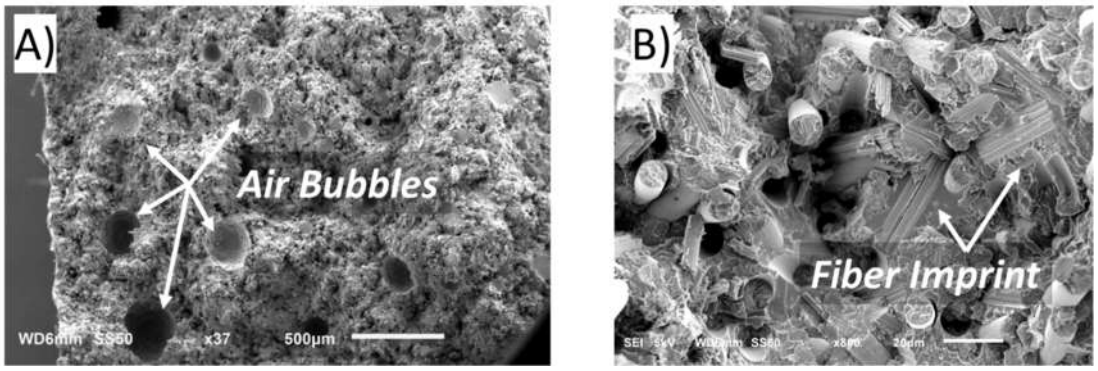

Figure. 3.5: *SEM images of the composites reinforced with 46% fibers. A) Low-magnification image showing the porosity, B) High magnification image showing the fiber orientation*

These fractographs show that the fibers are densely packed at high fiber loadings and that large porosities exist (Figure. 3.5A) within the composite specimens despite their unprecedentedly high mechanical strength and modulus. In other words, if these porosities or air bubbles are eliminated prior to the extrusion of the composite paste, the mechanical properties can be further enhanced.

In addition, the fibers show some alignment in the printing direction (perpendicular to the fracture plane). However, this alignment is significantly lower compared to those reported in the previous studies on 3D-printed carbon fiber polymer composites,[72, 82, 84, 90] where fibers with higher aspect ratios were utilized. SEM images of the composite specimens with different fiber volume fractions are shown in Figure. 3.6.

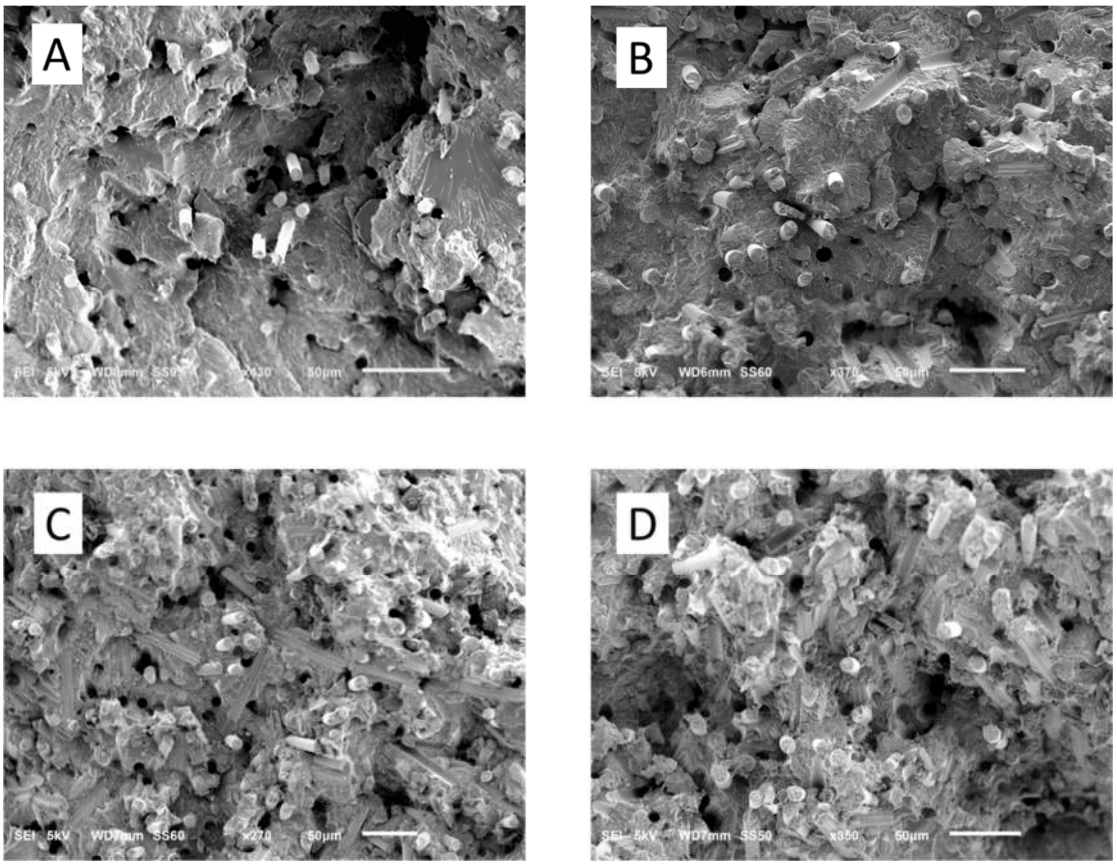

Figure. 3.6*: SEM images of the fracture surfaces for the longitudinally printed composite specimens at different fiber volumes A) 3%, B) 21%, C) 36%, D) 46%.*

The goal of 3D-printing short fiber reinforced composites at high fiber loading and high strength (Figure. 1.1) was achieved in this study. Manufacturing composite structures having high strength and stiffness (or modulus) at complex geometries will make a tremendous impact on various applications, most notably in aerospace, defense, and marine industries, because these materials offer lowered costs, ease of processing, higher chemical resistance, and most importantly reduced weights under similar strength requirements.

Figure. 3.7 represents the strength of the composite systems fabricated via direct write additive manufacturing as a function of their densities. The properties of the commonly used polymer materials (PLA, epoxy) and metals (aluminum and steel) are also marked in the figure for comparison.

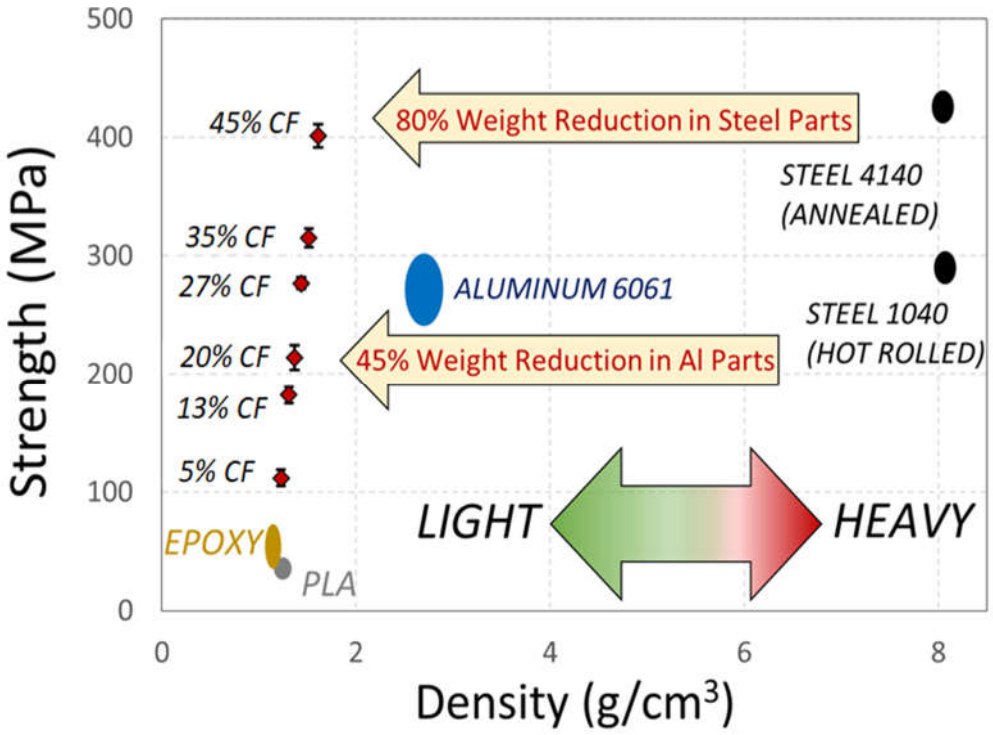

Figure. 3.7: *Comparison of strength versus density variation of the additively manufactured composites with the conventional polymers and metals.*

As the carbon fiber content is increased in the fabricated thermoset composites, the composite density showed a linearly increasing trend. Composites reinforced with 27% short fibers by volume had an equal strength to that of aluminum 6061 38 alloy, which is commonly used for aerospace, automotive, and marine applications. The density of this composite was, however, 45% lower than the density of aluminum. Therefore, the replacement of 6061 aluminum parts with additively manufactured thermoset composites can reduce their weights by nearly half.

More significant weight reduction can be achieved with higher fiber loading levels. Composites reinforced with 46% carbon fibers exceeded the yield strength of hot rolled steel 39 and matched the strength of annealed 4140 steel 40. Considering the densities of steel (8.05 g/cm^3) and the additively manufactured composite (1.6 g/cm^3) of this study, an 80% reduction in weight can be achieved if the steel parts are replaced with composite systems.

Elastic modulus of short fiber reinforced composites can be predicted by the well-known Halpin- Tsai analytical model. Assuming that all fibers are aligned perfectly in the printing direction, this model predicts the elastic modulus of the composite (*EC*) as follows:

$$E_C = \frac{(1+2s\eta_L f)}{1-\eta_L f} E_m \; where \; \eta_L = \frac{(E_r/E_m - 1)}{E_r/E_m + 2s} \tag{3.1}$$

where s is the aspect ratio for the fibers, f is the fiber volume ratio, and E_r and E_m are the elastic moduli of the fiber reinforcement and matrix, respectively. Strength of the short fiber reinforced composites (σ_C) can also be predicted using models described in [111, 112]. Unlike elastic modulus, critical aspect ratio (s_C) plays a significant role for estimating the composite strength. The ultimate strength of a material with aligned fibers is calculated as:

$$\sigma_C = \begin{cases} fs\,\dfrac{\sigma_m}{\sqrt{3}} + (1-f)\sigma_m, s < s_c \\ f\sigma_r\left(1 - \dfrac{\sigma_r\sqrt{3})}{4s\sigma_m}\right) + (1-f)\sigma_m, s \geq s_c \end{cases} \; where \; s_c = \frac{\sigma_r\sqrt{3}}{2\sigma_m} \tag{3.2}$$

where σ_m and σ_r are the matrix and the fiber (reinforcement) strengths, respectively. It should be noted that these analytical models are oversimplistic since they assume perfect alignment of the fibers in the longitudinal (printing) direction and neglect the distribution of the fiber length. A more detailed model exists [113] which accounts for the fiber orientation and size distribution. In addition, Halpin-Tsai model is more suitable for tensile properties of short fiber composites.

However, a recent study [84] has shown that flexural modulus are nearly identical to tensile elastic modulus and flexural stress is slightly (10-15%) higher than that the tensile strength for the short carbon fiber reinforced composites fabricated via direct write additive manufacturing.

Therefore, the flexural properties may be used as alternative to the tensile properties to understand the mechanical performance of these materials. Lastly, during 3-point bending tests, both tensile and compressive loading modes exist.

To validate that the fracture occurs under tension rather than the compression and the Halpin-Tsai equations (which are developed for tensile loading) are valid, compression tests were performed on the composite with the highest fiber volume ratio (46%). These tests revealed that compressive strength was 673.4±30 MPa which was much higher than the tensile strength (401 MPa) for the same fiber content.

Therefore, the assumption of the tensile failure during the 3-point bending tests are valid. Under these assumptions and considerations, Figure. 3.8 shows that the analytical model described by the Equations 3.1 and 3.2 underpredicts the strength and the modulus of the fabricated composites. In other words, composites fabricated in this work are significantly stronger (~4 times) and stiffer (~2 times) than the expected mechanical properties. Deviation between the predictions and the experimental data is in fact larger, in reality, because the analytical model assumes perfectly aligned fibers and, as the SEM images evidenced, the fibers are not well aligned in the longitudinal print direction. Therefore, if the fiber misalignment is included in the analytical model, the strength and modulus predictions would further reduce and the deviation between the analytical model and the experimental data would be larger.

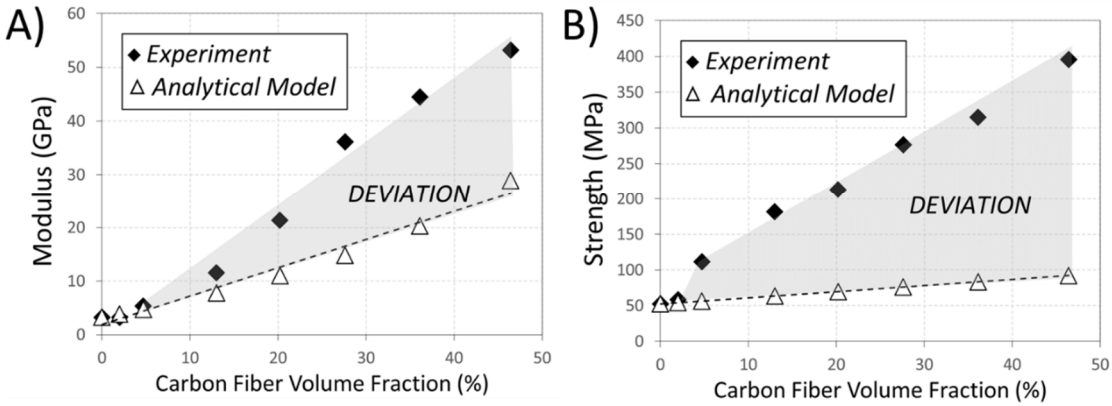

Figure. 3.8: *Comparison of the experimental data versus analytical model prediction for A) elastic modulus and B) ultimate strength*

Deviation between the predictions and the experimental data is larger for the case of strength. This is because the strength predictions are formulated based upon the critical aspect ratio for fiber reinforced composites. As Eq. 3.2 indicates, if the fiber aspect ratio is below the critical value, fiber tensile strength does not contribute to the strength of the composite. Critical aspect ratio depends on the fiber and matrix strengths and it was calculated to be s_c =80, which was significantly larger than the aspect ratio (s=4.5) for the milled fibers used in this study.

Existing studies claim that, if the fiber aspect ratio is significantly less than the critical value (s_c), the matrix deforms around the fiber such that there is virtually no stress transference and little reinforcement by the fiber [114]. So, why are the additively manufactured composites in this study much stronger than the predictions? How can these noticeably short fibers, nearly 20 times smaller than the required aspect ratio, reinforce the additively manufactured composites so effectively? Answers to these questions certainly require further exploration and additional research; however, we can obtain some clues about this peculiar behavior with more careful investigation of Figure. 3.8. This figure is redrawn with a close-up view of the lower fiber volumes in Figure. 3.9, below.

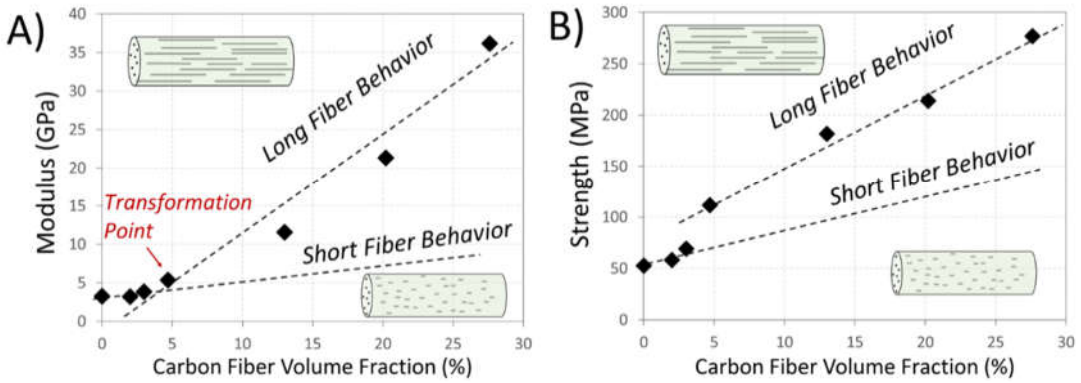

Figure. 3.9: *Effect of fiber loading on the reinforcement behavior of the carbon fibers. Two distinct fiber reinforcement behavior (short fiber, long fiber) were observed in A) modulus, B) strength.*

As this figure indicates, the analytical model predictions and the experimental data compare well at low fiber reinforcement levels and the fibers can minimally reinforce the composite as expected from the milled, short fibers. Above 5% fiber volume however, the strength and stiffness of the composites shift dramatically as a function of fiber volume fraction. After this critical fiber loading (~5%), which is marked as the transformation point on Figure. 3.9A, the fibers can reinforce the composite more effectively as if they act like longer reinforcements with high aspect ratios.

In both the modulus and strength plots shown in Figure. 3.9, a shift from short fiber behavior to longer fiber behavior was observed at the same saturation level (5%). This may be explained by the enhancement of the load transmittal zone, or reinforcement zone as shown in Figure. 3.10. The mechanical properties of the fiber-reinforced composites depend not only on the properties of the fiber and matrix, but also on the degree of load transmission from the matrix phase to the fibers. Interfacial adhesion between the fiber and the matrix phases and the length (or aspect ratio) of the fibers determine the level of load transmittance [114-117].

As shown in Figure. 3.10, under an applied load, the load transmittance from the matrix to the fiber is carried out mainly by the lateral surfaces. Therefore, if fiber matrix interface is weak (such as those in thermoplastic composites) or if the lateral fiber

surface is small (short fibers with low aspect ratios), load transmittance cannot be performed effectively. If the matrix is loaded with fibers above the saturation/transformation concentration (5%) as described in Figure 3.8, blue reinforcement zones might be overlapping and therefore fibers can distribute the force collaboratively as if they act together as a single, but longer, fiber with high reinforcement ability due to the strong cohesion in these zones. Below this threshold fiber concentration (5%), however, the matrix can deform around the fibers causing a reduction in strength and stiffness.

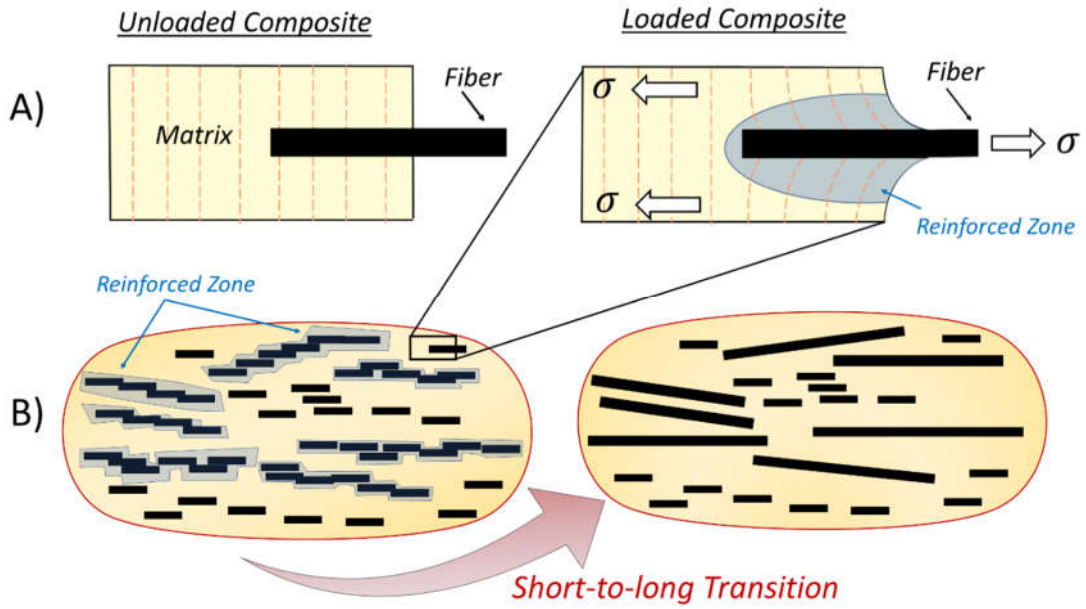

Figure. 3.10: *A) Schematic of load transfer between a short fiber and the polymer matrix under tensile loading. Red dashed lines show the change of displacements due to shear force between the matrix and the fiber. B) The proposed mechanism for the short to long fiber transformation at high fiber loading levels. Blue reinforced regions are only shown for the fibers with the overlapped reinforcement for clarity.*

To show additional evidence for the short-to-long fiber transformation, we fabricated composite specimens using unsized carbon fibers with the same length and aspect ratio. Since there is no sizing or chemical coupling between the fibers and the epoxy matrix, the interface between these phases is weaker and the reinforced zone is smaller in these

composites. In other words, we would not expect overlapped reinforcement zones nor short-to-long fiber transformation in these specimens.

As Figure. 3.11A indicates, the elastic moduli of these specimens were much lower than those fabricated with the sized fibers. In addition, the well-established Halpin-Tsai model well predicts the elastic moduli of these composite specimens for different levels of (5-36% by volume) fiber reinforcement. This is clear evidence that the only explanation for the higher elastic moduli of the composites prepared with sized fibers or strong matrix-fiber interface is the extended lengths of these fibers, or a pseudo fiber length transformation as described above. Similar to the elastic moduli measurements, the strengths of composites with unsized fibers were significantly lower than the sized fibers. Strength of these specimens, however, were higher than the predicted strengths calculated by Eqs. 3.1-3.2 as shown in Figure. 3.11B.

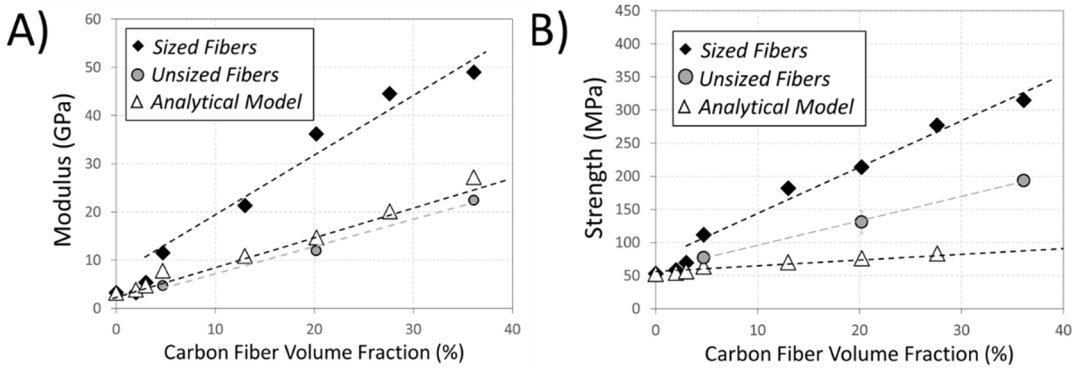

Figure. 3.11: *Comparison of the mechanical properties of the sized and unsized fiber reinforced composites to the analytical models A) Flexure Modulus, B) Flexure Strength.*

Higher strength of these composites can be explained by the high mechanical bonding between the fiber and the matrix phases provide high strength. To prove that mechanical bonding/latching exist even in the unsized fibers, we performed SEM analysis of the unsized fiber surface at high magnification.

Figure. 3.12A shows that similar to the sized fibers, unsized fibers had highly rough surfaces and this surface morphology significantly enhanced the adhesion to the epoxy matrix and therefore the pullout strength of these fibers. Fracture surfaces of the composites fabricated with unsized fibers in Figure. 3.12 B shows imprints of the fibers pulled out from the matrix which also indicate the strong adhesion between the carbon fibers and the epoxy matrix. This high adhesion was further enhanced in sized fibers with the chemical adhesion.

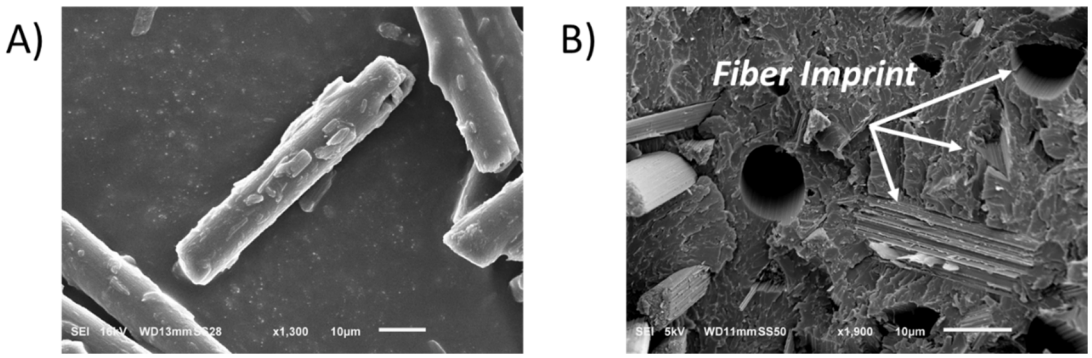

Figure. 3.12: *A) SEM image of the unsized fibers showing highly rough surface, B) Print marks of the unsized fibers on the fracture surface of the composite specimen indicating the strong adhesion between the carbon fibers and the epoxy matrix*

One of the key characteristics of additively manufactured fiber reinforced composites is that they are highly anisotropic. Strength and stiffness of these materials are significantly high in the printing direction while the mechanical performance is weak in all other orientations. This anisotropy greatly benefits the strength-to-weight ratio of fiber reinforced composites in the printing direction where fibers show maximum alignment.

However, it also limits their applications where high strength of materials is necessary in multiple loading directions. In order to assess the anisotropy of the short fiber reinforced composites, we performed mechanical tests on the specimens printed in the transverse orientation, where the weakest mechanical properties are expected.

In transversely printed specimens, the print lines extend perpendicular to the loading direction as shown in Figure. 3.13.

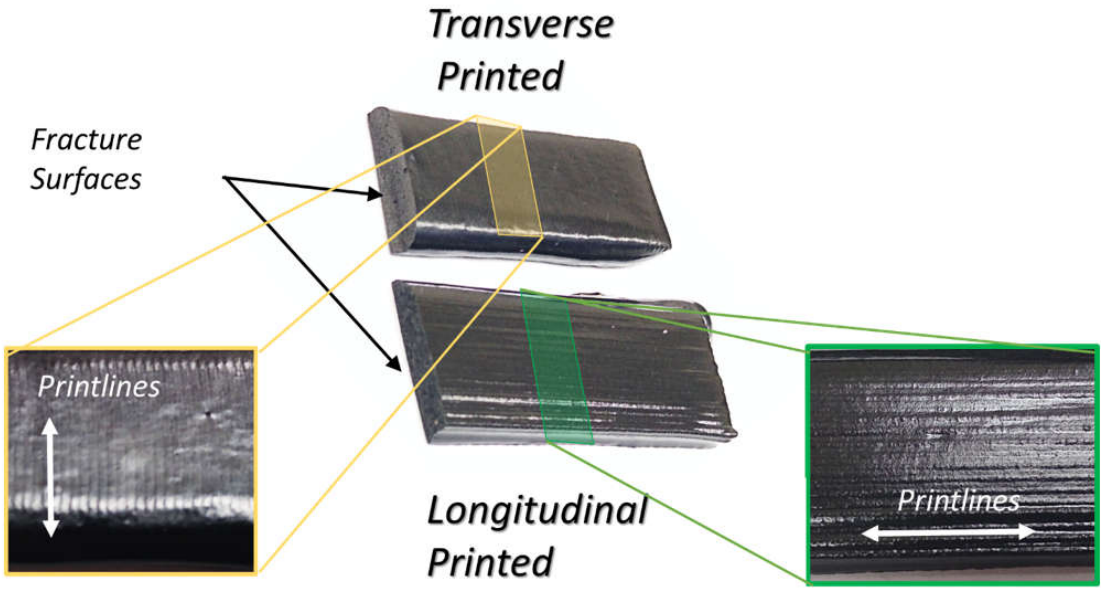

Figure. 3.13: *Images of the specimens fabricated in the longitudinal and transverse directions. Print lines are parallel to the bending stress (perpendicular to the fracture surface) in longitudinal printing. Print lines are perpendicular to the bending stress (parallel to the fracture surface in transverse printing).*

Figure. 3.14 shows the comparison of the flexure modulus and the strength of the specimens printed in the longitudinal and transverse orientations for three different fiber volume contents. As the figure indicates, the transverse properties were slightly lower than those measured in the longitudinal direction. The mechanical properties measured in longitudinal and transverse directions differed by less than 20% for the highest fiber loading (36%).

This anisotropy was far less than the previously reported [81] anisotropy level, where transverse properties were significantly (~70%) lower than those in the longitudinal direction.

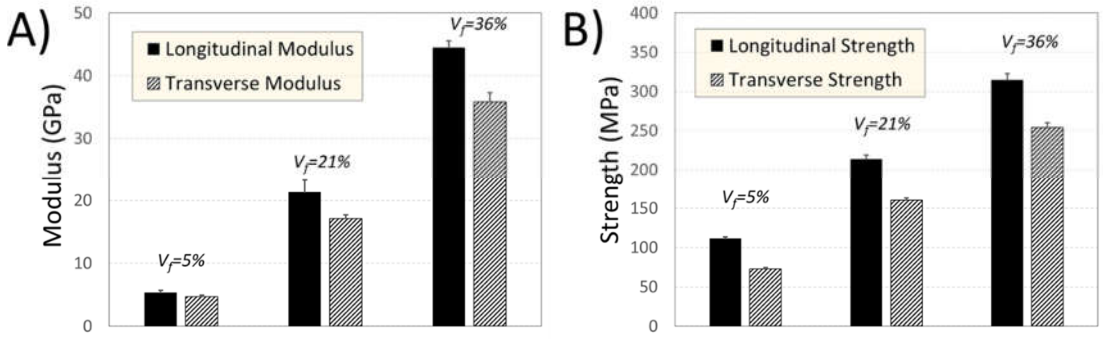

Figure. 3.14: *Anisotropy in the mechanical properties of the composites printed in longitudinal and transverse directions A) Flexure modulus comparison, B) Flexure strength comparison.*

Representative SEM images of the transversely printed specimens are given in Figure. 3.15. This figure shows the fibers which are weakly aligned in the transverse direction. Therefore, in both longitudinal and transverse printing directions, milled fibers with low aspect ratio showed less alignment under shear stress compared to the longer fibers preferred in the previous studies [84, 90] during the extrusion process and showed a higher level of mechanical isotropy.

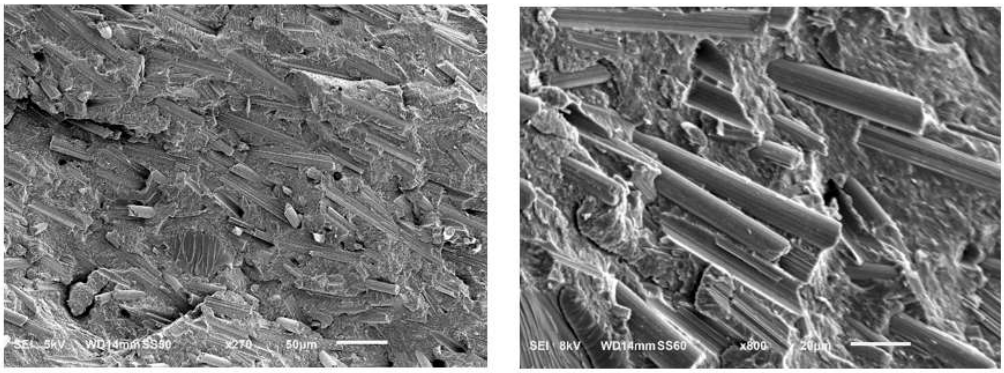

Figure. 3.15: *SEM images of the fracture surfaces for the transversely printed composite specimens. Fiber volume content is 36% by volume for the imaged specimen.*

In addition to flexural and compression tests, we performed fracture toughness tests as described in Chapter 2. As a quick review, this test was based on the ASTM D5528 - 01 Standard Test Method for Mode I. Three different sets according to fiber volume content was chosen to investigate the mechanical performance, namely, 0% (no carbon fiber), 15%, and 36%. All of the samples were printed in longitudinal direction (i.e. 0^0), and at least three samples were carried on in these experiments for each set. The average amount of the released energy (G_I) resulted from this test is presented in Table 3.1.

Table. 3.1: *Fracture toughness results in this study*

Fiber Volume Content %	Energy Released (N/mm)
0%	0.62
15%	0.44
36%	0.41

Results shows that the fracture toughness decreased by the addition of carbon fibers which is exactly the opposite results compared to the flexural and compression tests. After the analysis, we found out that a continuation in this test is possible. After reviewing some publications in the field, we realized that we could improve the fracture toughness by twisting the orientation of the layers in the 3D printing process (i.e., not depending on longitudinal direction only) to increase crack path and hence fracture toughness. To perform this, we formed two configurations in the 3D printing process, and we called them conf.1, and conf.2. To illustrate more, six different printing angles were used to fabricate the specimen. Figure. 3.17 shows the twisted angles in conf. 1. Likewise, Figure. 3.18 presents the conf.2 process.

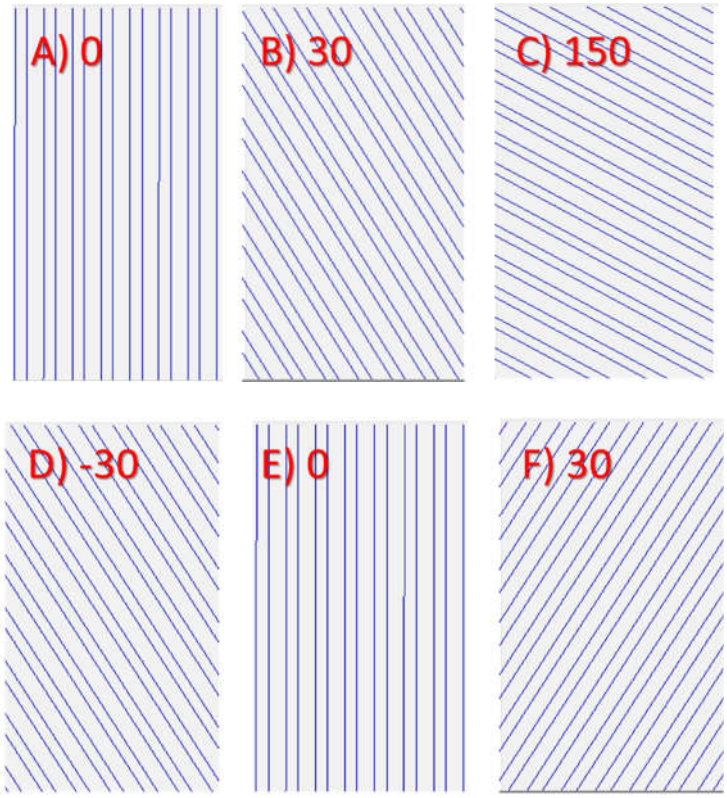

Figure. 3.16: *Configuration 1 (i.e. 6 Layers in different orientations)*

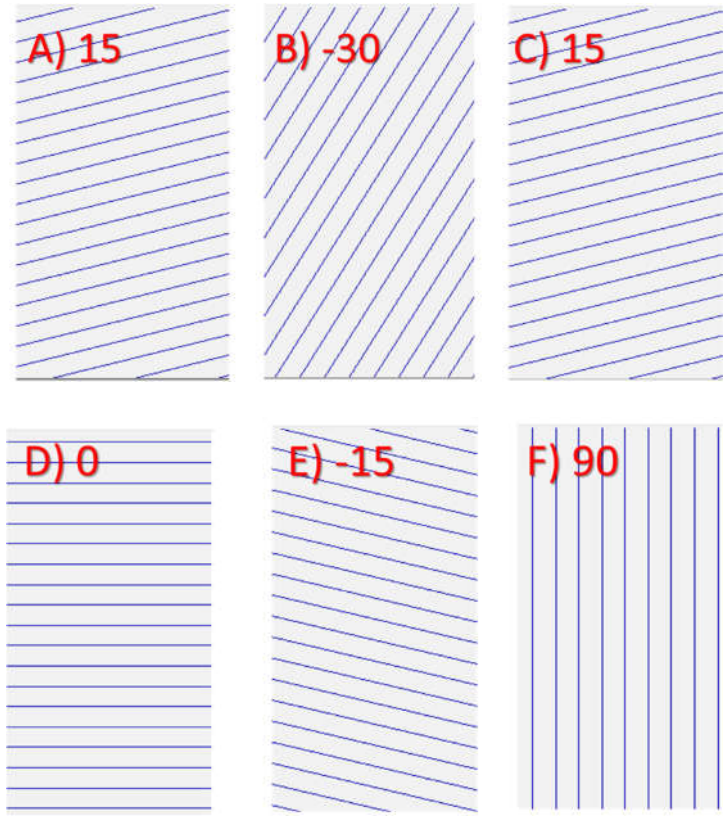

Figure. 3.17: *Configuration 2 (i.e. 6 Layers in different orientations)*

Using conf. 1 improved the fracture toughness by at least 35% compared to the longitudinal direction at the same fiber content. Also, 15 V_f % of carbon fibers were approximately enough to equate the energy released from the longitudinal direction as illustrated in Table 3.2. Figure. 3.18 represents the bar chart the results in the test. Also, Figure. 3.19 summarizes behavior of our created configurations after adding fibers.

Table 3.2: *The energy released from different orientations*

Fiber Content	Longitudinal	Conf. 1	Conf. 2
0%	0.62	N/A	N/A
15%	0.44	0.59	0.47
36%	0.41	0.54	0.40

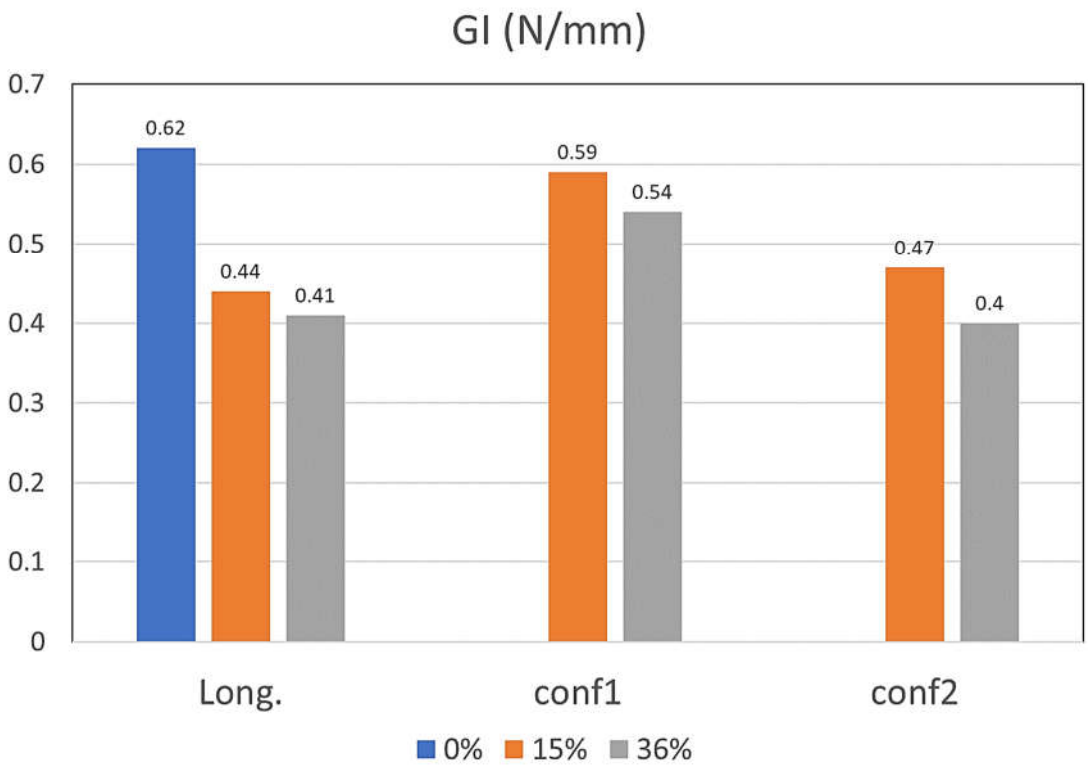

Figure. 3.18: *Fracture toughness test resulted values*

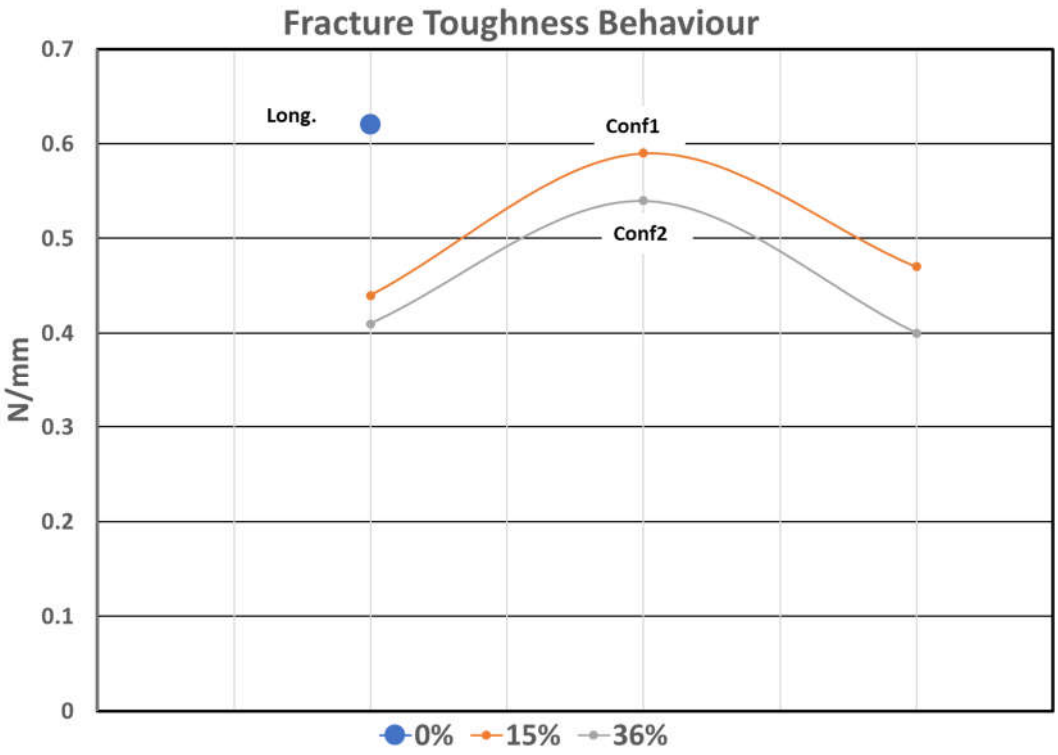

Figure. 3.19: *Fracture toughness behavior in terms of printing direction and carbon fibers contents*

3.5. Chapter Summary

In this chapter, we achieved the goal of developing high-strength, short fiber reinforced composites by direct write additive manufacturing. The compressive strength (σc = 400 MPa), flexural strength (σ_F = 400 MPa), and the flexural modulus (E=53GPa) of the fabricated composites far exceeded previously published results. This unprecedented mechanical performance was obtained by the ability to increase the fiber volume content from 5% to 46% with a customized direct write manufacturing system. Our extrusion system allowed printing of highly viscous composite inks without flow inconsistences and nozzle clogging issues.

Even at high fiber volume fractions, the results were unexpectedly high in comparison to the established mechanical models. This was due to the fact that the fibers used in

this study were milled fibers with low aspect ratios (much less than the calculated critical aspect ratio). The analytical models, however, predict that effective strength enhancement cannot be achieved using fibers having aspect ratios below the critical aspect ratio.

Our experimental results indicate that these models can successfully predict the experimental results at low fiber volume fractions. However, after a critical fiber volume level (V_f=5 %), fibers can strengthen the composites much more effectively, which may be explained by the overlapping reinforcement zones forming at close vicinity to the fibers. Due to the strong cohesion within these overlapping reinforcement zones, the load can be transferred collaboratively by multiple fibers. Therefore, a pseudo-transformation from a short fiber to long fiber can explain the enhanced strength of these materials systems at higher fiber loadings.

In addition to the improved mechanical performance of additively manufactured composites in the longitudinal direction, mechanical properties were nearly as good in the weakest, transverse direction. Considering the high strength and stiffness, material isotropy, low cost and flexibility of fabrication, additively manufactured short carbon-fiber reinforced composites will find a wide range of applications in the near future. These materials have the potential to replace ubiquitous structural metals, such as aluminum and low-strength steels, and therefore create tremendous weight savings. The mechanical properties of these materials can be further enhanced by optimizing the additive manufacturing parameters and reducing the defects due to a significant amount of bubbles present in the existing specimens.

Compression tests evidenced eliminating these defects will significantly enhance the mechanical performance of these composite structures. Voids may be created during the mixing process in air or manual transfer of the mixed ink into the printing cartridge.

These voids/bubbles can be eliminated by mixing the inks under vacuum and automated ink transfer reducing the risk of bubble introduction into the printing material. These strategies to further improve the mechanical properties of the composites will be further investigated in our future studies. In addition, if the alignment of short fibers can be improved by optimizing the printing process parameters, the improved fiber alignment will further enhance the strength and modulus of the composite materials along the longitudinal direction and maximize anisotropy.

CHAPTER 4: ADDITIVE MANUFACTURING OF DUCTILE KEVLAR FIBER THERMOSET COMPOSITES

Kevlar fibers stand out as these uniquely reinforcements that combining low density, high strength and high ductility. Additive manufacturing of short Kevlar fiber-reinforced thermoset composites is however rather difficult as these fibers cannot be broken down or milled unlike glass or carbon fibers due to their high flexibility. Despite from the availability of continuous unidirectional Kevlar fibers, short Kevlar fibers are not commercially available. This chapter evidences the robust developed method to produce short Kevlar fibers, and explains in detail how these fibers are implemented in the AM of reinforced thermoset composites for the first time. Consequently, improvement of strength, modulus as well as the elongation at break using the Kevlar fibers validating the unique mechanical performance of these composite systems.

4.1. Kevlar Fibers in This Research

Kevlar fibers used in this research are from ‘’Aramid Uni-web’’ Kevlar fibers family. Uni-Web Aramid Fiber is an innovative fiber type reinforcement that consists of a ply containing non-woven unidirectional aramid fibers. Web of polymer fibrils can maintain fibers connectivity position by a fine web that rest on the surface. The fibril or web system enables the fabric to be formed efficiently, cropped, or slice, providing clear-cut edges. Consequently, it will remain to lie flat and straight and cannot move or shift during the cutting process.

The main reasons for using these fibers are common in their less dense, light weight, high toughness, and high ductility that they have compared to other fibers. In addition to that, Kevlar fibers are compatible with many matrix materials like epoxy resins and is proper for usage in resin infusion manufacturing. These novel qualities give it an extraordinary performance in composite reinforcements applications. Figure 4.1 represents a continuous sheet of these fibers.

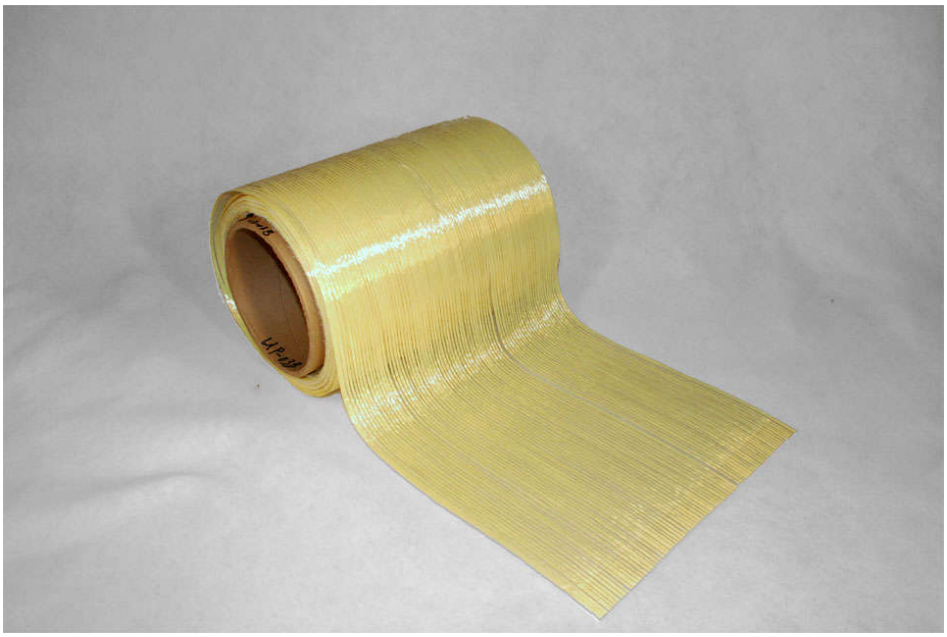

Figure. 4.1: *Aramid unidirectional Kevlar fibers [118]*

4.2. Preparation of Short Kevlar Fibers by Laser Cutting Process

The process of cutting continuous, unidirectional Kevlar fibers (Uniweb, ACP Composites) with 15-micron diameter was carried out by using a laser cutter system (Universal Laser Systems VLS 2.30). The cut fibers were then sieved in order to avoid uncut parts of the Kevlar sheet and to remove the unseparated fiber bundles. The length of cut fibers was selected to be 800 microns to minimize the burning effects of laser at the cut regions (at each ends) of the fibers. JOEL JSM-6010 PLUS/LA scanning electron microscope (SEM) was used to observe the morphology of the Kevlar fibers after the cutting and sieving processes were completed. Prior to imaging process, a gold

layer of (1-2 nm) thickness was sputter coated on the surface of the fibers. Figure 4.2A represents the fibers after the cutting process showing the consistency of the fiber lengths. This figure also shows the separated, single fibers as well as the fiber bundles in which fibers are not completely separated. Figure 4.2B shows the close-up view of the imaged Kevlar fibers.

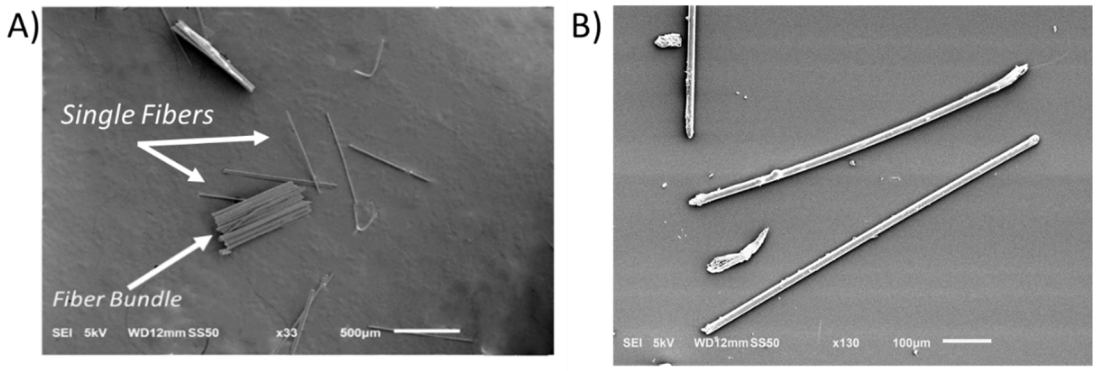

Figure. 4.2: *SEM Image of Kevlar fibers used in this study.*

4.3. Rheology Characterization

The preparation of Kevlar fiber based composite ink material was started similar to the ink preparation method used in Chapter 3. The process has started by adding Garamite-7305 nanoclay from BYK additives into epoxy resin (EPON Resin 826 from Hexion) to be used as rheology modifiers. Following this step, cut Kevlar fibers were added into the epoxy-nanoclay mixture systematically until reaching the maximum volume of Kevlar fibers. As the Kevlar fiber content was increased in the composite ink mixture, the amount of nanoclay was gradually reduced to keep the viscosity at a similar level since the Kevlar fiber addition also increased the viscosity of the ink.

The nanoclay content corresponding to the Kevlar fiber amounts of 0% (base ink), 3.5% and 6.3% were obtained as 10%, 7% and 5.5%, respectively. Finally, 5% (ppm of epoxy) latent curing agent from Sigma-Aldrich (1- Ethyl-3-methylimidazolium

dicyanamide) was added to the mixture. Planetary shear mixer (Thinky ARE-310) was used for 3 minutes at a speed of 2000 rpm to obtain homogeneous ink mixture.

Rheological properties of all samples were characterized using a Discovery HR-2 Rheometer (TA Instruments, New Castle, DE). Testing geometry was set up on an 8 mm flat plate with a gap height of 500 μm. Prior to each test, samples were subjected to a 1-minute conditioning phase at a constant shear rate of 0.1 s^{-1} followed by a 2-minute rest period for reformation of the ink structure. Viscosity of the samples was measured as a function of shear rate by sweeping through controlled shear rates (0.004-19 s^{-1}).

4.4. 3D Printing of the Kevlar Ink Using Direct Write Method

Extrusion of the prepared ink was preformed through a 2 mm nozzle with a printing speed of 40 mm/s using the same customized displacement controlled direct write extrusion setup used in the previous chapter. This system allows the extrusion of highly viscous composite inks loaded with high volume of fiber reinforcement. Nozzle clogging at high fiber loadings was resolved by using the integrated vibration motors which shake the nozzle and avoid clogging with accumulated fibers.

The build plate of the 3D printer was covered with a Teflon sheet before the printing process in order to prevent the adhesion between the printed specimens and the build plate and easy removal of the cured specimens. The printing process was performed at room temperature, and the curing process of the printed specimens was carried out inside an oven for 15 hours at 100^0C. Specimens were 3D printed in rectangular prism shapes according to the flexural test standards explained in next section.

4.5. Mechanical Characterization

Mechanical characterization of the 3D printed specimens was assessed by performing 3-Point bending tests of both static and dynamic (fatigue) loading. Sample geometries defined in ASTM D7264/D7264M− 07 standard (Standard Test Method for Flexural Properties of Polymer Matrix Composite Materials) were used to run both test types. Additionally, span-to-thickness ratio was kept 16:1 for all created samples, and to ensure the validity of this ratio, the span length was tuned for each specimen before executing the tests.

Figure 4.3 depicts the schematic for the fatigue test workflow which was performed on a servo-hydraulic test machine and characterized by a maximum loading capacity of 10 kN.

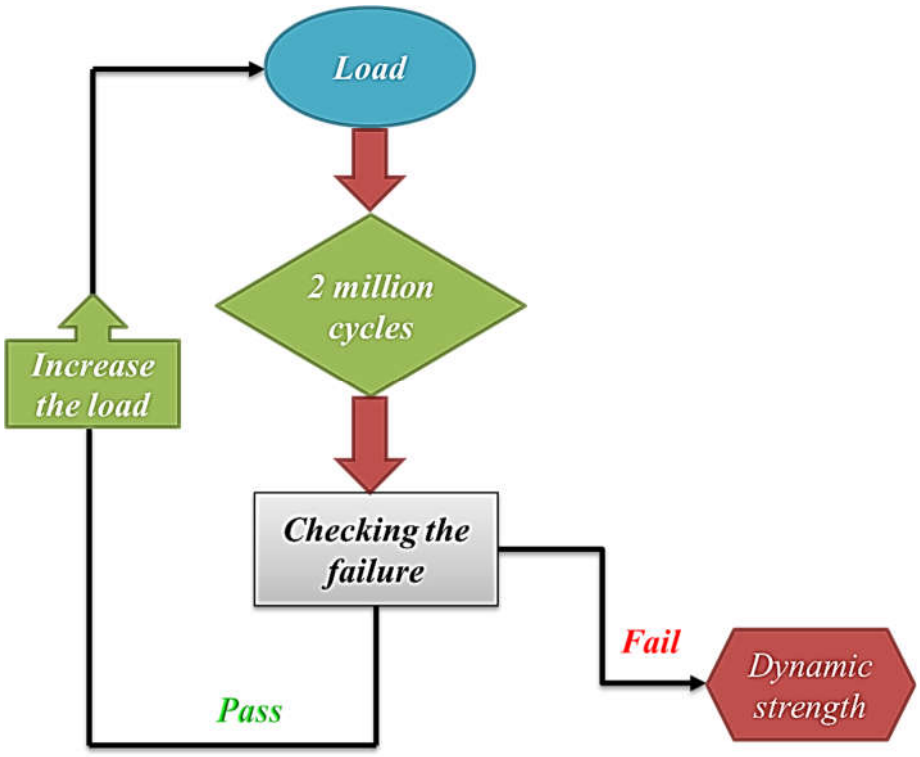

Figure. 4.3: *The workflow of fatigue characterization*

The system was tested under load control, applying a sinusoidal wave load with a frequency of 7 Hz at a load ratio, R (Minimum Load/ Maximum Load), of 0.1. The cyclic stresses are normally well below the yield strength of the material. Therefore, the level of the maximum load for the first test was taken as 50 % of the average yield load for each group and the tests were terminated after exceeding the 2 million cycles. If specimen failed before the runout cycle, the load was decreased until the desired run out cycle was achieved for the next specimens. If the specimen did not fail in 2 million cycles, then the load level was increased gradually, and the dynamic testing was repeated. This process (testing/load level increase) continued until the material failure was reached. The material failure was defined as the point when the load on the specimen dropped below the load level which is 25 % of the initial load value.

At least 4 samples were tested to quantify the standard deviation and validate the repeatability of the mechanical tests. For all mechanical test measurements, student's T-test statistical analysis was performed to quantify the statistical significance between the results. Significance was defined as the low p-value ($p<0.05$) according to the T-tests.

4.6. Results and Discussion

Viscosity measurements on the printing inks are given in Figure 4.4. This figure indicates that the neat epoxy showed the minimum viscosity having the range of 15-38 Pa. s throughout the entire shear rate spectrum. Addition of the nanoclay and Kevlar fibers were both found to be very effective in terms of modifying rheology and enhancing the viscosity by nearly 3 orders of magnitude as shown in this figure. Maximum viscosity was observed in highly loaded Kevlar fibers (6.3%) in which medium amount (7%) of nanoclay was used to optimize the viscosity.

All inks showed different levels of shear thinning behavior. Shear thinning was minimal in the neat epoxy compared to all other composite inks (epoxy/nanoclay or epoxy/nanoclay/Kevlar) which showed significant level of shear thinning (nearly 3 orders of magnitude).

As described previously [119], shear thinning is a desired property used in direct ink writing process in which viscous inks undergo a high level of shear within extrusion nozzles and transform from highly viscous solid to low-viscosity liquid state. As the material is extruded, it retains its shape transforming back to a viscous, solid state.

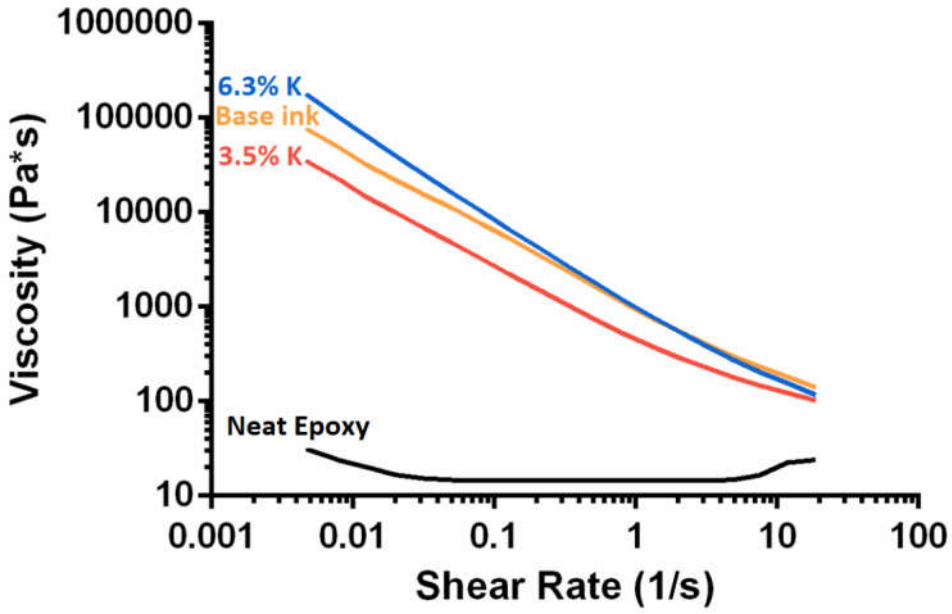

Figure. 4.4: *Rheology measurement of the ink used in this study.*

Static flexural strength, and static flexural modulus results of the additively fabricated Kevlar fiber reinforced composites at different fiber volume fractions (0%, 3.5% and 6.3%) are given in Figure 4.5A and Figure 4.5B, respectively. Both flexural strength and flexural modulus showed gradual increase as the fiber content is increased within the composite.

Maximum strength of 108 MPa was achieved for the highest Kevlar volume content of 6.3% which marks %105 increase compared to the unfilled base ink as shown in Figure 4.5A.

Maximum flexural modulus was achieved to be 4.3 GPa for the flexural modulus at maximum Kevlar content marking 39% increase in modulus compared to that of the base ink.

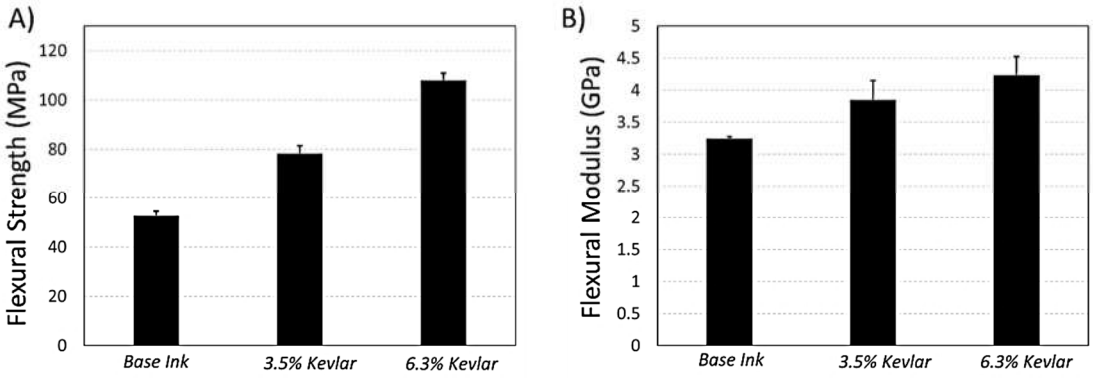

Figure. 4.5: *Flexure strength and flexure modulus variation of additively manufactured Kevlar-fiber reinforced composites as a function of fiber loading levels.*

Flexural strain at break measurements of 6.3% Kevlar fibers exceeded that of the base ink by 96% due to the higher ductility of Kevlar fibers as shown in Figure 4.6.

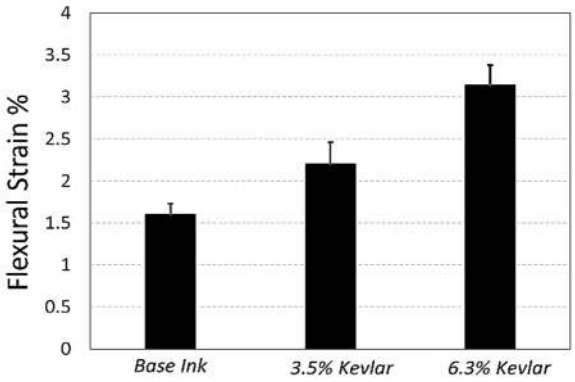

Figure. 4.6: *Strain variation as a function of fiber loading levels.*

Unlike the stiffer glass and carbon fibers, Kevlar fibers significantly enhance the ductility of the epoxy/nanoclay composite which can lead to unique applications of 3D-printed composites such as those requiring high energy absorption, impact resistance and high toughness.

SEM images of the fractural cross-sections of Kevlar composite specimens are shown in Figure 4.7. These images display that Kevlar fibers have homogeneous distribution within the composite, and they are well-aligned in the printing direction indicated by the perpendicular orientation along the fracture surface.

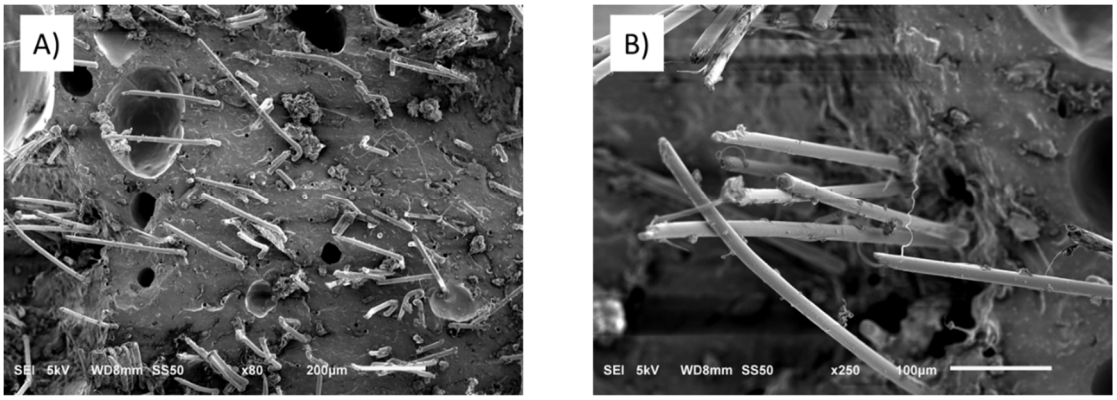

Figure. 4.7: *SEM images of the fractured surface of Kevlar reinforced composites*

In addition, it is clearly shown that Kevlar fibers demonstrate deformable, ductile behavior in these images which can explain the dramatic enhancement in failure strain. SEM figures also show that the direct write printing leads to strong adhesion between the print layers in contrast to the FFF process since the different print layers are not distinguishable in these images. High porosity, however, is visible in terms of different sizes of voids which will be further evaluated in the next section.

Table 4.1 summarizes the static mechanical testing results for the short Kevlar reinforced epoxy composites. In the table, previously reported flexure test results for Kevlar/ABS [120] and Kevlar/Nylon [46] thermoplastic composites are also given.

The comparison indicates that flexural strength and modulus are higher than the short Kevlar fiber reinforced ABS studied previously. However, it must be noted that, in this reference study, the printing was performed in two orientation ($0^0/90^0$) which may lower the strength and modulus in the longitudinal direction.

Comparison of our results with additively manufactured, continuous Kevlar reinforced Nylon composites shows that continuous Kevlar leads to slightly higher strength and modulus enhancement compared to short Kevlar/epoxy composites investigated in our study.

Considering the much lower volume of Kevlar fibers (6.3%) compared to the continuous Kevlar fiber reinforced composites (10%), and the fiber length is much smaller (~800 microns), it is remarkable to achieve comparable mechanical properties. This unprecedented mechanical performance of additively manufactured short Kevlar fiber reinforcement might be due to the strong adhesion and wetting between the short Kevlar fibers and the epoxy matrix.

In addition, although porosity is present, interlayer porosity is not shown in the fabricated samples as assessed by the SEM images shown above which may play a role in enhancement of static mechanical performance of these composites.

Table 4.1: *Mechanical performance comparison of Kevlar fibers in both thermoplastic and thermoset matrices*

Sample Name	Fiber Type	Print Direction	Fiber Volume Fraction	Flexural Strength (Mpa)	Flexural Modulus (GPa)	Flexural Strain (%)
Base ink (This Study)	-	0°	-	52.63 ± 1.94	3.24 ± 0.13	1.18 ± 0.02
Kevlar/Epoxy (This Study)	Short	0°	3.5	78.30 ± 1.38	3.84 ± 0.31	0.71 ± 0.03
Kevlar/Epoxy (This Study)	Short	0°	6.3	108 ± 13.37	4.52 ± 0.29	0.83 ± 0.03
Kevlar/ABS [120]	Short	0°/90°	4.42	45.50 ± 0.66	1.62 ±0.04	N/A
Kevlar/Nylon [46]	Continuous	0°	10	125.80±3.27	6.65 ±0.23	N/A

To investigate fatigue strength of short Kevlar fiber-reinforced composites, rectangular flexure test specimens were prepared which are similar to those used for static flexural tests. Figure 4.8 A shows the fatigue strength measurements in terms of number of cycles (S-N curve), and Figure 4.8 B represents the average values of the fatigue strength measured at 2 million cycle for each set.

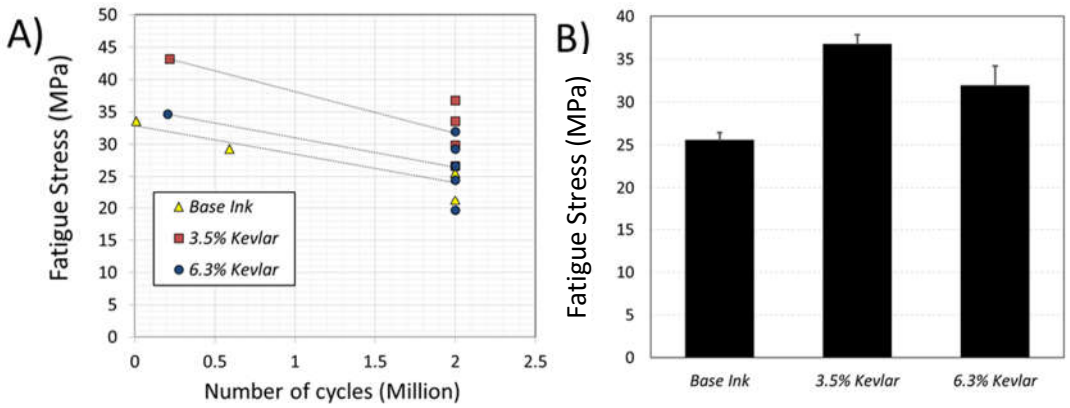

Figure. 4.8: *Dynamic fatigue strength of additively manufactured composites as a function of number of load cycles.*

It was expected that the highest fatigue strength would be obtained from the reinforced specimens that have the largest content of Kevlar fibers similar to what was observed in static flexural tests. However, it was seen that the highest recorded fatigue strength values were obtained in the 3.5% of Kevlar fibers samples, where a notable improvement was observed for this set compared to the other sets. Standard deviation shown in Figure 4.8B indicates that the increase of fatigue strength in 3.5% Kevlar fiber reinforced composite compared to the base ink and decrease of this strength as more fibers (6.3%) were added into the composite were statistically significant. Compared to the base ink, 3.5% Kevlar reinforced specimens showed 43% increase in fatigue strength. Increasing the fiber content to 6.3% resulted in 15 % decrease in the strength compared to the 3.5% Kevlar reinforced composites.

So, why is the dynamic (fatigue) strength of the additively manufactured, highly loaded fibers in this study weaker than the expectations? Why is the fatigue strength maximum at medium level (3.5%) Kevlar fiber reinforcement? Although answers to these questions certainly need more investigations and additional research, we can get have some clues about this strange material behavior from the optical microscope images in Figure 4.9.

Figure 4.9 shows 3 different sections of the polished cross-sectional surfaces of each set (base ink, 3.5% Kevlar and 6.3% Kevlar). These images indicate that as the Kevlar fiber volume is enhanced, porosity is enhanced as well. Figures 4.9 G-H show that increase in porosity is significant at the high (6.3%) Kevlar concentration.

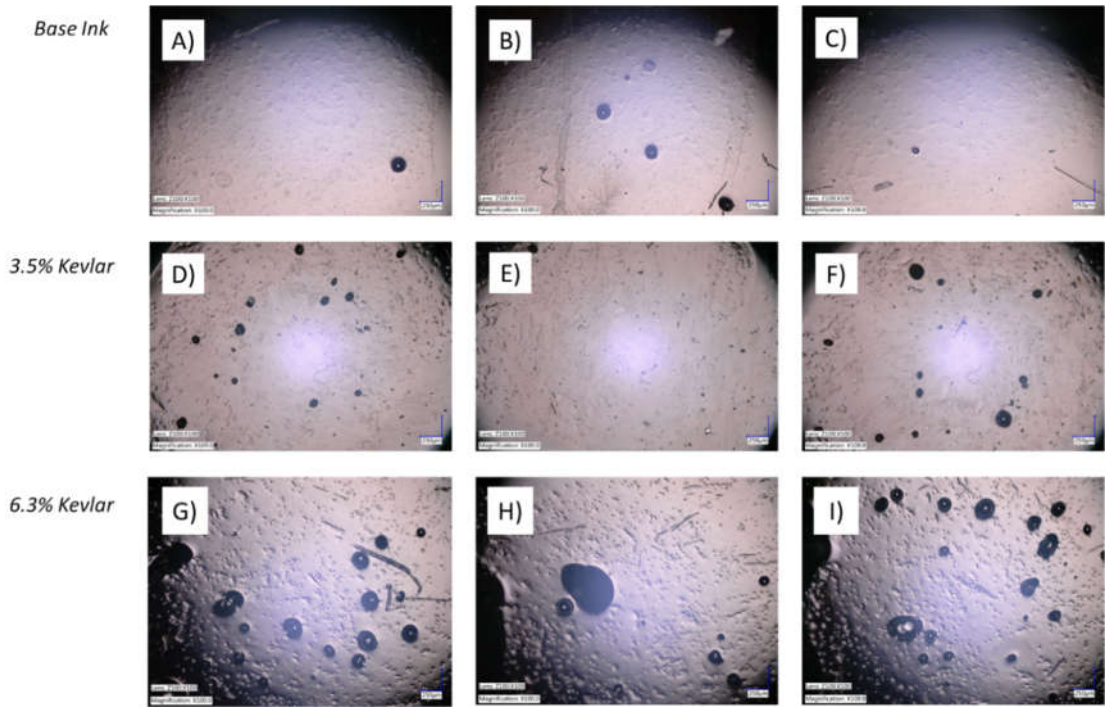

Figure. 4.9: *Optical microscope images of the dynamic fractured surface of Kevlar reinforced composites in this study*

Image analysis was conducted on the images in Figure 4.9 quantifying the porosity. The porosity measurement values performed on the specimens used for the dynamic flexure testing are provided in Table 4.2. According to this table, porosity increases from 1.39% to 2.05% and finally 12.04% as the Kevlar volume fraction was enhanced from 0% to 3.5% and 6.3%. Therefore, the loss of the fatigue strength at highly loaded Kevlar composites could be explained by the increase of the porosity in these specimens. Such pores can act as crack initiation sites and result in premature failure in cyclic loading. In static testing however, the high strength of Kevlar reinforcement surpassed the adverse effects of these voids on the flexural strength and therefore static strength continued increasing as more fibers were added within the composite as summarized in Table 4.2.

Table 4.2: *Static and Fatigue flexural strength and the porosity of additively manufactured composites*

Sample Name	STATIC Flexural Strength (Mpa)	FATIGUE Flexural Strength (Mpa)	Porosity on the fracture surface (%)
Base ink	52.63 ± 1.94	3.24 ± 0.13	1.39
Kevlar 3.5%	78.30 ± 1.38	3.84 ± 0.31	2.05
Kevlar 6.3%	108 ± 13.37	4.52 ± 0.29	12.04

4.7. Chapter Summary

Kevlar fiber reinforcement provides unique advantages compared to glass and carbon fibers due to their lightweight and high ductility. In this work, additive manufacturing of short Kevlar fiber reinforced thermoset composites were examined.

Vibration-integrated; direct write additive manufacturing methodology was utilized to fabricate Kevlar reinforced printing inks. Composite inks were fabricated by laser cutting of continuous fibers and mixing the cut short fibers with epoxy and rheology modifying nanoclay.

Custom-made direct write additive manufacturing setup allowed us to achieve the highest volume (6.3%) of Kevlar reinforcement within thermoset composites up to date. Static and dynamic mechanical properties of these composites were characterized by performing flexure tests.

Enhancement in flexural strength, flexural modulus as well as failure strain were obtained in Kevlar reinforced specimens compared to the base ink structure. Static flexural strength and modulus of 108 MPa and 4.3 GPa were attained for 6.3% Kevlar fiber reinforced composites, respectively.

Dynamic test results showed that cyclic loading significantly reduced the flexural strength of the additively manufactured samples. In addition, it was observed that addition of 3.5% Kevlar fibers enhanced the fatigue strength but further addition of fibers to 6.3% resulted in reduction in fatigue strength.

The lowered strength of 6.3% of Kevlar fiber reinforced samples can be explained by the presence of higher defect density and porosity in these samples, and future efforts are needed to further enhance the Kevlar loading and reduce the porosity to maximize both the static and dynamic mechanical properties of additively manufactured, Kevlar reinforced composites. In addition, manufacturing process needs enhancement to obtain better separation of the Kevlar bundles which will further increase the mechanical performance and help achieve the use of full reinforcement potential of the short Kevlar fibers.

CHAPTER 5: ADDITIVE MANUFACTURING OF SYNTACTIC FOAM LIGHTWEIGHT THERMOSET COMPOSITES

This chapter aims to investigate the AM of thermoset-matrix syntactic foams using direct write methodology for the first time. Syntactic foams with high strength and temperature resistivity which cannot be achieved via thermoplastic matrix were obtained successfully. The effects of short carbon fiber reinforcement on the mechanical performance of syntactic foams got a point of interest in further enhancing the mechanical performance. Therefore, a novel methodology for preparation of thermoset-matrix syntactic foams and syntactic foam composites via DW manufacturing is reported in this chapter.

5.1 Ink characterization

The process of preparing syntactic foam printing material started by mixing epoxy resin (EPON Resin 826 from Hexion) and glass microspheres (3M, K20) with a median diameter of 60 μm and density of 0.2 g/cc^3. Glass microspheres were added into epoxy matrix in gradual amounts until the desired volume fraction was achieved. Glass microspheres increased the viscosity of epoxy acting as a rheology modifier and the printed composites retain their shape after deposition on the substrate. To enhance mechanical strength, short carbon fibers (K6371M, 50 μm long, 11 μm diameter acquired from Mitsubishi Chemical Carbon Fiber and Composites, USA) were added at desired amounts to the epoxy-glass microsphere mix.

As a control, base ink epoxy samples without carbon fiber or glass microspheres were fabricated. Garamite-7305 nanoclay from BYK additives were used as rheology modifiers instead of glass microspheres.

For the preparation of each ink (base ink, glass microsphere ink and glass microsphere/carbon fiber ink), a planetary shear mixer (Thinky ARE-310) was used for 3 minutes at a speed of 2000 rpm to assure the homogeneity of the resulted mixtures. As the last step, latent curing agent (hardener) from Sigma-Aldrich (1- Ethyl-3-methylimidazolium dicyanamide) was added and mixed for 1000 rpm for 1 minute.

5.2. Direct Write 3D Printing of the Syntactic Foam Inks

Depositing the syntactic foam ink material was performed using the same customized displacement controlled direct write extrusion setup that was explained in detail in the previous chapters. However, composite inks were dispensed this time through 640 microns tapered nozzles at printing speed of 40 mm/s.

Also, prior to the printing process, the build plate was coated with a Teflon sheet, which prevented the adhesion between the specimen and the build plate and enabled easy extraction of the cured parts. The printing process was performed under room temperature, and the fabricated samples were cured inside an oven for 15 hours at 100 ^{0}C.

In addition to printing test samples for mechanical testing, specimens in triangular lattice structures were also fabricated. Slic3r open source software was utilized to convert solid prisms into triangular lattice structures by specifying 20%, 30% and 40% infill densities. These slicing operations allowed fabrication of 3 different lattice structures with varying triangular cell densities.

5.3. Morphology and Density Characterization

Size and spheroidicity of the as received microspheres were observed using JOEL JSM-6010 PLUS/LA scanning electron microscope (SEM). A thin (1-2 *nm*) gold layer was sputter coated on the surface of the microspheres before imaging. Representative image of the glass microspheres is shown in Figure 5.1.

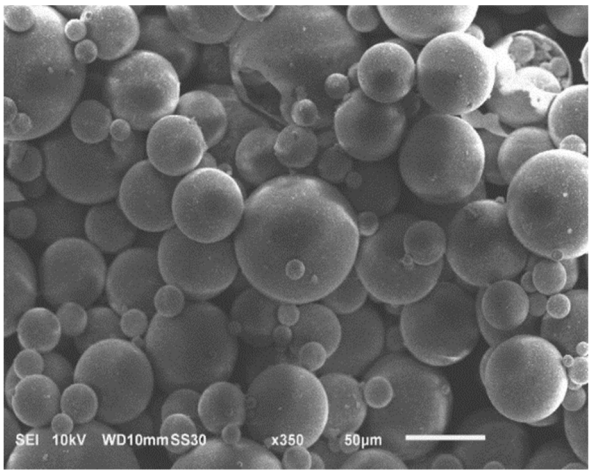

Figure. 5.1: *SEM Image of glass microspheres used in this study.*

SEM was also used to image fracture surfaces of the specimens after mechanical tests were performed. Density of the fabricated specimens were calculated by measuring the specimen volumes and masses. At least four samples were analyzed for each set of samples to validate the accuracy in density measurements.

5.4 Mechanical Characterization

Mechanical performance of the printed specimens was measured using Instron universal testing machine performing both 3-Point bending and compression tests. 3-Point bending tests were performed in accordance with ASTM D7264/D7264M− 07 standard (Standard Test Method for Flexural Properties of Polymer Matrix Composite Materials). 16:1 span-to-thickness ratio was employed where the span length was

adjusted for each sample to keep this ratio valid in 3-Point bending test. For compression tests, ISO 604 (Plastics-Determination of compressive properties) standard was followed. For both mechanical testing procedures, at least four tests were executed for each set of samples to provide the repeatability and quantify the experimental variability.

5.5. Results and Discussion

Figure 5.2 represents the three specimens fabricated for the flexure testing; base ink (epoxy matrix and clay nanoparticles), syntactic foam (epoxy filled with glass microspheres) and carbon fiber reinforced syntactic foam.

Figure. 5.2: *3D printed flexure test specimens*

Average densities for all specimens are given in Table 5.1. Filling epoxy resin with 60% hollow glass microspheres reduced the epoxy density by nearly 40% achieving 0.71 g/cc^3 buoyant density in glass microsphere syntactic foams (GSF). Adding 15% carbon fiber and 56% glass microspheres resulted the density of 0.83 g/cc^3 which was 14% higher compared to using only glass microspheres fillers.

Table. 5.1: *Density measurements of the fabricated solid and lattice specimens*

Sample Name	Glass Microsphere (%)	Carbon Fiber (%)	Density (g/cc^3)
Base ink	0	0	1.18 ± 0.02
Glass Syntactic Foam (GSF)	60	0	0.71 ± 0.03
Glass/Fiber Syntactic Foam (GFSF)	56	15	0.83 ± 0.03

Flexural and compressive strengths of the syntactic foams are given in Figure 5.3A in comparison with the nanoclay filled base ink. As the figure indicates, both flexural and compressive strengths of the glass microsphere filled syntactic foams were lower than those of the base ink. However, adding 15% carbon fiber in GFSF specimens enhanced the compressive strength of the syntactic foams to nearly match that of the base ink. This increase was more dramatic in flexural strength measurements where the flexural strength of GFSF exceeded that of the base ink. Compressive strengths of all composites were significantly higher than their tensile strengths since the defects such as voids as well as glass microspheres create stress intensification and act as crack initiation locations under tensional loading, thereby reducing their strength. Under compression, the voids collapse without adversely affecting the fracture strength.

During flexure testing, specimens underwent both tension and compression and fail earlier under lower loads compared to those under purely compressive loads.

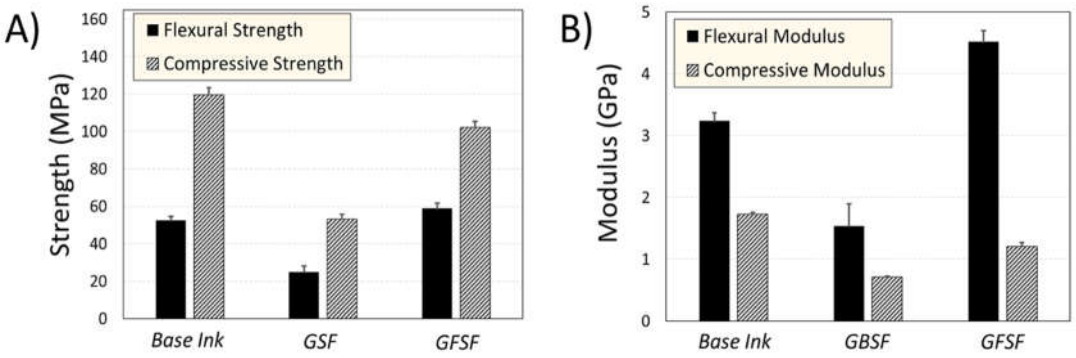

Figure. 5.3: *Flexure strength versus flexure modulus variation of additively manufactured carbon-fiber reinforced composites as a function of fiber loading levels.*

Figure 5.3B shows the flexural and compressive modulus of the syntactic foam and the base ink specimens. Similar to the strength, modulus of the GSF specimens were found to be lower than the base ink and it was enhanced by the addition of carbon fibers. However, modulus under compressive loading was significantly lower than the flexural modulus of the syntactic foam.

Stiffer response of syntactic foams under tensile loading compared to compression was reported in a previous study [121] where microsphere wall thickness and porosity were found to be important parameters determining the compressive stiffness. Error bars in the bar plots illustrates the standard deviation where Student T-test was used to perform the statistical significance. All results showed significant variation according to T-test ($p<0.05$).

Figure 5.4A and 5.4B show the SEM micrographs of the syntactic foams at different magnifications after flexural testing was performed. It is clear from Figure 5.4A that, voids exist in the printed thermoset syntactic foam.

The voids in the printing ink might have formed during the mixing of the material or manual transfer of this material from the mixer to the printing cartridge. Figure 5.4C shows the SEM image of the fiber reinforced, thermoset syntactic foam. Short carbon fibers are visible around the hollow microspheres.

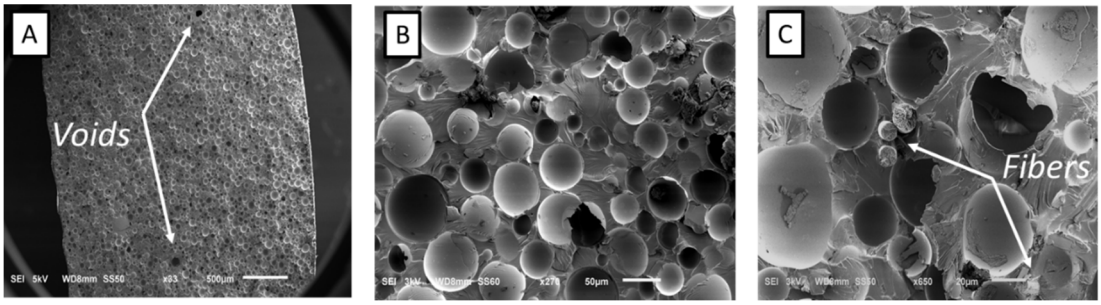

Figure. 5.4: *SEM images of the fractured surface of A-B) glass syntactic foam (GSF) and C) Fiber reinforced glass syntactic foam (GFSF)*

5.6. Additive Manufacturing of Ultra-Lightweight Lattice Syntactic Foam Structures

In Figure 5.5, the carbon fiber filled syntactic foam printed in triangular lattice structure is shown which indicates the ability of the direct ink system to fabricate syntactic foams in complex geometries.

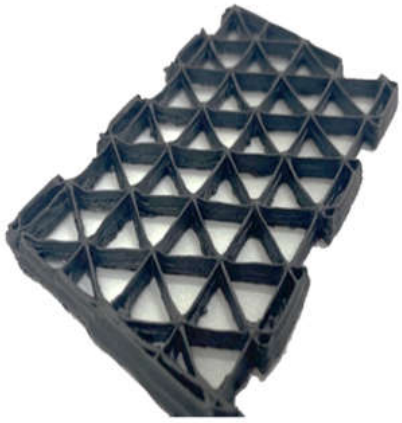

Figure. 5.5: *3D printed, fiber reinforced lattice structure*

Lattice structures were fabricated using the carbon fiber reinforced syntactic foams (GFSF) in triangular lattice orientation as shown above. Three lattice cell densities were created by altering the infill density of in the slicing procedure as described previously. Infill densities of 20%, 30% and 40% resulted in the densities of 0.42 g/cc^3, 0.49 g/cc^3 and 0.54 g/cc^3, respectively in these ultra-lightweight structures.

To investigate mechanical properties of ultra-light syntactic foams, carbon fiber-reinforced foam material was 3D printed into triangular lattice structure with different cell densities. Figure 5.6A and 5.6B shows strength and modulus measurements of these foams under compressive loading. Images on each bar in these figures represents the sliced CAD model to show the relative cell densities under different infill amounts. Figure 5.6A indicates that lattice structure becomes stronger as the infill ratio is increased. Similarly, modulus data show the same increasing behavior as the cell density and the infill ratio is increased.

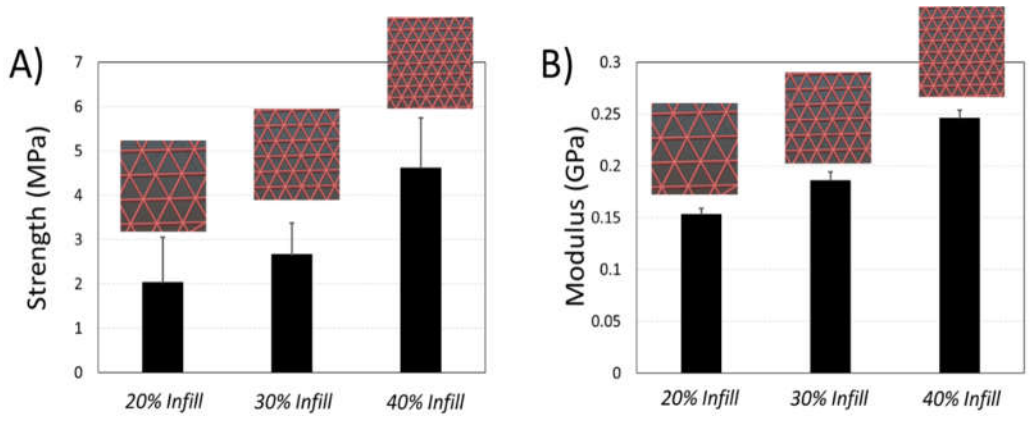

Figure. 5.6: *A) Stress Comparison B) Modulus Comparison*

The mechanical properties of all the solid and lattice structures obtained in flexural and the compression tests are summarized in Table 5.2 below. It should be noted that only compression tests were performed on the lattice structures since the compression is the most common loading type for the components consisting of lattice structures such as sandwich panels.

Table. 5.2: *Flexural and compressive mechanical properties of additively manufactured composites.*

Sample Name	Flexural Strength (MPa)	Flexural Modulus (GPa)	Copmressive Strength (MPa)	Compressive Modulus (GPa)
Base ink	52.63 ± 1.94	3.24 ± 0.13	119.63 ± 3.77	1.73± 0.03
Glass Syntactic Foam (GSF)	25.03 ± 3.06	1.54 ± 0.36	53.25 ± 2.59	0.716 ± 0.01
Glass/Carbon Syntactic Foam (GFSF)	58.87 ± 2.85	4.52 ± 0.18	102.29 ± 3.11	1.21 ± 0.06
20% Infill-Lattice (GFSF-L)	-	-	2.04 ± 1.01	0.15 ± 0.006
30% Infill-Lattice (GFSF-L)	-	-	2.67 ± 0.71	0.19 ± 0.0008
40% Infill-Lattice (GFSF-L)	-	-	4.62 ± 1.12	0.25 ± 0.007

To compare the compressive mechanical performance of the fabricated composites to the previously published results on syntactic foams, Ashby charts are generated in Figure 5.7. This figure indicates that mechanical strength and stiffness of the fabricated syntactic foams are significantly (>5 folds) higher than those reported previously for additively manufactured thermoplastic syntactic foams. This increase is more dramatic in fiber reinforced thermoset syntactic foams in which fibers significantly increased strength and stiffness of the foams.

Comparison of the carbon fiber reinforced thermoset composites investigated in this study to the glass fiber reinforced epoxy syntactic foams [122] show that similar compressive modulus values are achieved.

However, additively manufactured carbon fiber reinforced syntactic foams have lower density and higher strength compared to the glass fiber reinforced foams which were cast into molds. Compressive modulus and strength of lattice syntactic foams are also shown in Figure 5.7. For these structures, mechanical properties can be predicted using well established scaling laws [119, 123]. Hence elastic modulus of the fiber reinforced syntactic foam structures is written in terms of elastic modulus of the solid material (GFSF) and the densities of the solid and the lattice material.

$$\frac{E_L}{E_S} = \frac{1}{3}\left(\frac{\rho_L}{\rho_S}\right) \tag{5.1}$$

Similarly, strength of the lattice parts can be written as a function of solid material strength and the densities of the solid and the lattice material. Strength modeling is based on two distinct cell wall failure types as shown in Equations 5.2 and 5.3 below: compression/tension or elastic buckling.

Tension/Compression: $$\frac{\sigma_L}{\sigma_S} = \frac{1}{3}\left(\frac{\rho_L}{\rho_S}\right) \tag{5.2}$$

Elastic Buckling: $$\frac{\sigma_L}{\sigma_S} = \frac{1}{3}\left(\frac{\rho_L}{\rho_S}\right)^2 \tag{5.3}$$
)

Prediction of elastic modulus in Figure 5.7A is in well agreement with the experimentally measured data. However, the analytical model overestimates the strength of the lattice syntactic foams. This is mainly due to the defects of the syntactic foams including the porosity, missing print lines and the discontinuous print lines as shown in SEM images in Figure 5.8. It must be noted that the adverse effects of these defects are more significant in the lattice structures compared to the solid specimens since the effective surface area carrying the load is much smaller in the lattice components and therefore the defects are more detrimental.

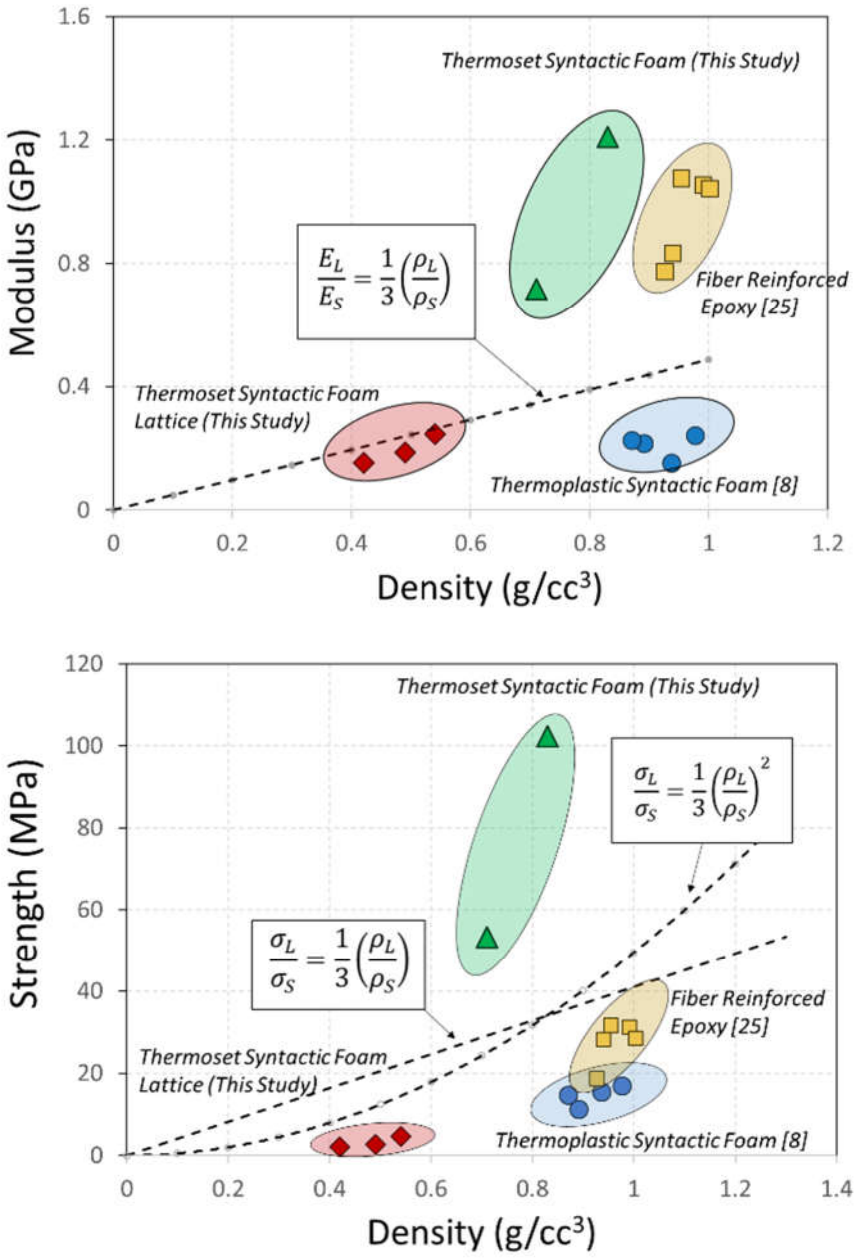

Figure. 5.7: *Ashby charts summarizing the mechanical property variation of the syntactic foams under compressive loads, A) Elastic modulus, B) Strength*

SEM micrographs of the triangular lattice in Figure 5.8 also indicate that there is an overlap of the print lines at the intersection (joint) points of the lattice. This overlap is a as result of the triangular pattern generated by the sliced CAD model, and it is unavoidable using the current printing methodology.

These overlapped roads at the joints may not be desirable for dimensional accuracy, however, it may highly beneficial for the structural integrity of the lattice structures since these points are the weakest locations and depositing extra material at the junctions will help enhancement of the mechanical performance. as an evidence to this strength enhancement, failure in the middle of the cell wall was observed rather than the fracture of the junction as shown in Figure 5.8.

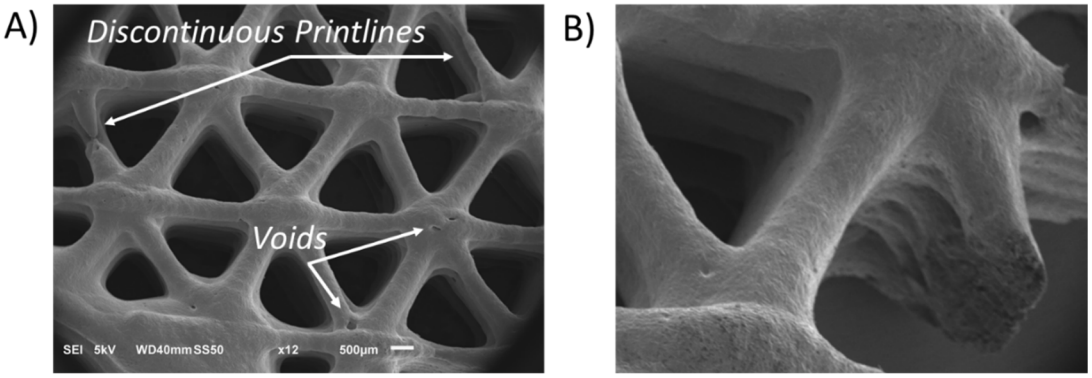

Figure. 5.8: *SEM micrographs of the triangular lattice structures A) Defects in the printed lattice structure (Mag:12X), B) Fracture at the cell wall of the lattice structure (Mag:27X)*

5.7. Chapter Summary

This study explored the direct write additive manufacturing of lightweight thermoset based syntactic foams in complex geometries. Compression and flexure tests performed on the fabricated samples revealed that additively manufactured thermoset based syntactic foams are significantly stronger and stiffer than the thermoplastic foams.

In addition, mechanical properties of these foams can be tailored by reinforcing these foams with short carbon fibers to achieve the desired mechanical performance.

Lattice structures with reduced densities were successfully fabricated via direct write additive manufacturing. However, strengths of these structures were found to be lower than the expected values, due to the defects existing within the printed material. Voids

are the main sources of this imperfections which affect the continuity of the printing and the mechanical performance of the lattice structures. Voids may be created during the mixing process or manual transfer of the mixed ink into the printing cartridge. These voids/bubbles can be eliminated by performing mixing under vacuum and automated ink transfer reducing the risk of bubble introduction into the printing material. These strategies to further improve the mechanical properties of the solid as well as lattice structures will be further investigated in our future studies.

Syntactic foams are unique material systems with reduced density, high impact resistance and high specific strength. In this study, we outlined a novel methodology to fabricate these materials in complex geometries. Scaling up of this technology to achieve component scale fabrication and eliminating the existing defects by optimizing the printing parameters and maximizing the mechanical performance will further facilitate the adoption of these materials in wider range of applications in various fields including marine, automotive and aerospace industies.

CHAPTER 6: CONCLUSION AND FUTURE WORK

This thesis summarizes the 3-year long research efforts on the additive manufacturing of short chopped fibers thermoset composites. Delta bot 3D printer was modified to print several types of composite specimens reinforced with deposited chopped fibers. Two types of fibers were used. However, in the initial stages, the base ink material (pure epoxy and clay with no fiber enhancements) was 3D printed successfully to have it as a reference for mechanical performance comparison purposes after the addition of fibers.

The pure epoxy was mixed with chopped carbon fibers from Mitsubishi company, namely, pitch carbon fibers. The average size of the fibers is about 50 microns. The main purpose of using these fibers is to enhance the strength performance of the composite materials since these fibers are strong and stiff. In the state- of the- art studies, it was found out that it is difficult to add more than 5% by volume from the fibers to the additively fabricated ink mixture. However, a developed 3D printing method was used to add 46% of these fibers as a volume fraction for the first time in this research. Vibration integrated motors are used on the nozzle outlet to shake the material during the 3D printing process in order to achieve this volume fraction. Printing using 46% of these fibers gave us unprecedented high mechanical performance (strength (>400 MPa), stiffness (53GPa)) compared to the previously studies.

In addition, second type of fibers were used to enhance ductility property of the composite structures. To achieve that, Kevlar fibers from Aramid Uni-web Kevlar fibers family were used. These fibers are less in dense, light in weight, and have high ductility compared to other fibers. However, it was challenging to find commercial

short chopped Kevlar fibers because they are not commercially available. Despite from this, a method using laser cutting machine was developed to cut the continuous sheets of Kevlar fibers. As a result, short chopped fibers were successfully produced with consistent length of 800 μm. Using our developed 3D printing technique, we could add 6.3% V_f from these fibers to enhance the ductility of the produced composites. The ductility of the resulted composite has been increased by two folds compared to the base ink material.

As a third goal in this research, syntactic foam materials were additively manufactured in thermoset resin for the first time. We could add about 60% by volume of glass-microspheres to produce ultra-lightweight composites. The mechanical performance of these structures was better than the additively manufactured syntactic foam thermoplastic composites. Using our extrusion set up, we could supply the syntactic foam-based composite with 15% of carbon fibers as a volume fraction to even further enhance the mechanical performance of the resulted structures.

The mechanical performance of all fabricated structures in this thesis was investigated using three-point bending test, compression test, and fracture toughness test. Also, Hierarchical microstructures of the additively fabricated specimens were imaged using scanning electron microscopy to observe the artefacts such as porosity, infill and material interdiffusion, which are inherent drawbacks of the 3D printing process. Regarding the future work of this work, we can claim that existing studies have failed so far to give sufficient consideration to 3D printed hybrid structures based on the thermoset resins. It might be difficult for the first sight to create tall structures using thermoset resins. This is due to the fact that thermoset resins do not have sufficient yield strength to balance the gravitational forces and keep its shape after certain numbers of 3D printed layers.

Thorough these drawbacks, however, some researchers started to develop some initial ideas and methods to solve these issues, and I strongly recommend prolonging this research trying to have a progress in this field (i.e., hybrid structures). A second point I would like to mention as a further future work is the porosity issue. SEM images in this research proved the existence of air voids. Despite from this fact, we exceeded the most up to date recorded mechanical performance in additive manufacturing of short fiber thermoset composites. What I see is the ability of this research to be extended furthermore to find methods in order to eliminate the air voids from the fracture surfaces. Consequently, the mechanical performance can be further enhanced.

References

1. Guo, N. and M.C. Leu, *Additive manufacturing: technology, applications and research needs.* Frontiers of Mechanical Engineering, 2013. **8**(3): p. 215-243.

2. Kianian, B., S. Tavassoli, and T.C. Larsson, *The role of additive manufacturing technology in job creation: an exploratory case study of suppliers of additive manufacturing in Sweden.* Procedia CIRP, 2015. **26**: p. 93-98.

3. Lutz, F. and R.W. Phillips, *A classification and evaluation of composite resin systems.* Journal of Prosthetic Dentistry, 1983. **50**(4): p. 480-488.

4. Fan, C., R. Ott, and T. Hufnagel, *Metallic glass matrix composite with precipitated ductile reinforcement.* Applied Physics Letters, 2002. **81**(6): p. 1020-1022.

5. Reifsnider, K., *Modelling of the interphase in polymer-matrix composite material systems.* Composites, 1994. **25**(7): p. 461-469.

6. Gialeli, C., A.D. Theocharis, and N.K. Karamanos, *Roles of matrix metalloproteinases in cancer progression and their pharmacological targeting.* The FEBS Journal, 2011. **278**(1): p. 16-27.

7. Kim, K.-Y. and L. Ye, *Interlaminar fracture toughness of CF/PEI composites at elevated temperatures: roles of matrix toughness and fibre/matrix adhesion.* Composites Part A: Applied Science and Manufacturing, 2004. **35**(4): p. 477-487.

8. Singh, J., D. Singh, and M. Sutaria, *Ceramic composites: roles of fiber and interface.* Composites Part A: Applied Science and Manufacturing, 1999. **30**(4): p. 445-450.

9. Zahl, D.B. and R. McMeeking, *The influence of residual stress on the yielding of metal matrix composites.* Acta Metallurgica et Materialia, 1991. **39**(6): p. 1117-1122.

10. Park, S.-J., M.-K. Seo, and J.-R. Lee, *Roles of interfaces between carbon fibers and epoxy matrix on interlaminar fracture toughness of composites.* Composite Interfaces, 2006. **13**(2-3): p. 249-267.

11. Vaughan, T. and C. McCarthy, *Micromechanical modelling of the transverse damage behaviour in fibre reinforced composites.* Composites Science and Technology, 2011. **71**(3): p. 388-396.

12. Wang, C., et al., *Effect of carbon fiber dispersion on the mechanical properties of carbon fiber-reinforced cement-based composites.* Materials Science and Engineering: A, 2008. **487**(1-2): p. 52-57.

13. Kalaprasad, G., K. Joseph, and S. Thomas, *Influence of short glass fiber addition on the mechanical properties of sisal reinforced low density polyethylene composites.* Journal of Composite Materials, 1997. **31**(5): p. 509-527.

14. Mishra, S., et al., *Studies on mechanical performance of biofibre/glass reinforced polyester hybrid composites.* Composites Science and Technology, 2003. **63**(10): p. 1377-1385.

15. Jayaraman, K. and D. Bhattacharyya, *Mechanical performance of woodfibre–waste plastic composite materials.* Resources, Conservation and Recycling, 2004. **41**(4): p. 307-319.

16. Caramaro, L., et al., *Morphology and mechanical performance of polyphenylenesulfide carbon fiber composite.* Polymer Engineering & Science, 1991. **31**(17): p. 1279-1285.

17. Ci, L. and J. Bai, *The reinforcement role of carbon nanotubes in epoxy composites with different matrix stiffness.* Composites Science and Technology, 2006. **66**(3-4): p. 599-603.

18. Tjong, S.C. and Z. Ma, *Microstructural and mechanical characteristics of in situ metal matrix composites.* Materials Science and Engineering: R: Reports, 2000. **29**(3-4): p. 49-113.

19. Ramasubramaniam, R., J. Chen, and H. Liu, *Homogeneous carbon nanotube/polymer composites for electrical applications.* Applied Physics Letters, 2003. **83**(14): p. 2928-2930.

20. Holbery, J. and D. Houston, *Natural-fiber-reinforced polymer composites in automotive applications.* Jom, 2006. **58**(11): p. 80-86.

21. Windhorst, T. and G. Blount, *Carbon-carbon composites: a summary of recent developments and applications.* Materials & Design, 1997. **18**(1): p. 11-15.

22. Leng, J., et al., *Shape-memory polymers and their composites: stimulus methods and applications.* Progress in Materials Science, 2011. **56**(7): p. 1077-1135.

23. Das, T.K. and S. Prusty, *Graphene-based polymer composites and their applications.* Polymer-Plastics Technology and Engineering, 2013. **52**(4): p. 319-331.

24. Pommet, M., et al., *Intrinsic influence of various plasticizers on functional properties and reactivity of wheat gluten thermoplastic materials.* Journal of Cereal Science, 2005. **42**(1): p. 81-91.

25. Carvalho, A.J., *Starch: major sources, properties and applications as thermoplastic materials*, in *Monomers, polymers and composites from renewable resources*. 2008, Elsevier. p. 321-342.

26. Ryokawa, H., et al., *The mechanical properties of dental thermoplastic materials in a simulated intraoral environment.* Orthodontic Waves, 2006. **65**(2): p. 64-72.

27. Kohda, N., et al., *Effects of mechanical properties of thermoplastic materials on the initial force of thermoplastic appliances.* The Angle Orthodontist, 2013. **83**(3): p. 476-483.

28. McGee, S.H., *Curing characteristics of particulate-filled thermosets.* Polymer Engineering & Science, 1982. **22**(8): p. 484-491.

29. Torres, A., et al., *Recycling by pyrolysis of thermoset composites: characteristics of the liquid and gaseous fuels obtained.* Fuel, 2000. **79**(8): p. 897-902.

30. Kouparitsas, C., et al., *Recycling of the fibrous fraction of reinforced thermoset composites.* Polymer Composites, 2002. **23**(4): p. 682-689.

31. de Luzuriaga, A.R., et al., *Epoxy resin with exchangeable disulfide crosslinks to obtain reprocessable, repairable and recyclable fiber-reinforced thermoset composites.* Materials Horizons, 2016. **3**(3): p. 241-247.

32. Palmer, J., et al., *Successful closed-loop recycling of thermoset composites.* Composites Part A: Applied Science and Manufacturing, 2009. **40**(4): p. 490-498.

33. Jahandideh, A. and K. Muthukumarappan, *Star-shaped lactic acid based systems and their thermosetting resins; synthesis, characterization, potential opportunities and drawbacks.* European Polymer Journal, 2017. **87**: p. 360-379.

34. Pickering, S.J., *Recycling technologies for thermoset composite materials—current status.* Composites Part A: Applied Science and Manufacturing, 2006. **37**(8): p. 1206-1215.

35. Sreenivasan, S., et al., *Recent developments of kenaf fibre reinforced thermoset composites.* Materials Research Innovations, 2013. **17**(sup2): p. s2-s11.

36. Leibler, L., J.-P. Pascault, and S. Ritzenthaler, *Thermoset materials with improved impact resistance*. 2005, Google Patents.

37. Ma, S. and D.C. Webster, *Degradable thermosets based on labile bonds or linkages: A review.* Progress in Polymer Science, 2018. **76**: p. 65-110.

38. Yu, K., et al., *Reprocessing and recycling of thermosetting polymers based on bond exchange reactions.* Rsc Advances, 2014. **4**(20): p. 10108-10117.

39. Zhang, Y., et al., *Malleable and recyclable poly (urea-urethane) thermosets bearing hindered urea bonds.* Advanced Materials, 2016. **28**(35): p. 7646-7651.

40. Moulton, S.E. and G.G. Wallace, *3-dimensional (3D) fabricated polymer based drug delivery systems.* Journal of Controlled Release, 2014. **193**: p. 27-34.

41. Ngo, T.D., et al., *Additive manufacturing (3D printing): A review of materials, methods, applications and challenges.* Composites Part B: Engineering, 2018. **143**: p. 172-196.

42. Bettini, P., et al., *Fused deposition technique for continuous fiber reinforced thermoplastic.* Journal of Materials Engineering and Performance, 2017. **26**(2): p. 843-848.

43. Caminero, M., et al., *Interlaminar bonding performance of 3D printed continuous fibre reinforced thermoplastic composites using fused deposition modelling.* Polymer Testing, 2018. **68**: p. 415-423.

44. Chabaud, G., et al., *Hygromechanical properties of 3D printed continuous carbon and glass fibre reinforced polyamide composite for outdoor structural applications.* Additive Manufacturing, 2019. **26**: p. 94-105.

45. Chacón, J., et al., *Additive manufacturing of continuous fibre reinforced thermoplastic composites using fused deposition modelling: effect of process parameters on mechanical properties.* Composites Science and Technology, 2019. **181**: p. 107688.

46. Dickson, A.N., et al., *Fabrication of continuous carbon, glass and Kevlar fibre reinforced polymer composites using additive manufacturing.* Additive Manufacturing, 2017. **16**: p. 146-152.

47. Justo, J., et al., *Characterization of 3D printed long fibre reinforced composites.* Composite Structures, 2018. **185**: p. 537-548.

48. Striemann, P., et al., *Compression testing of additively manufactured continuous carbon fiber-reinforced sandwich structures.* Materials Testing, 2018. **60**(9): p. 801-808.

49. Vaneker, T., *Material extrusion of continuous fiber reinforced plastics using commingled yarn.* Procedia CIRP, 2017. **66**(ISSN 22128271): p. 317-322.

50. Yu, T., et al., *Tensile and flexural behaviors of additively manufactured continuous carbon fiber-reinforced polymer composites.* Composite Structures, 2019. **225**: p. 111147.

51. Oztan, C., et al., *Microstructure and mechanical properties of three dimensional-printed continuous fiber composites.* Journal of Composite Materials, 2019. **53**(2): p. 271-280.

52. Van Der Klift, F., et al., *3D printing of continuous carbon fibre reinforced thermo-plastic (CFRTP) tensile test specimens.* Open Journal of Composite Materials, 2016. **6**(01): p. 18.

53. Goh, G.D., et al., *Characterization of mechanical properties and fracture mode of additively manufactured carbon fiber and glass fiber reinforced thermoplastics.* Materials & Design, 2018. **137**: p. 79-89.

54. Friedrich, K. and A.A. Almajid, *Manufacturing aspects of advanced polymer composites for automotive applications.* Applied Composite Materials, 2013. **20**(2): p. 107-128.

55. Soutis, C., *Fibre reinforced composites in aircraft construction.* Progress in Aerospace Sciences, 2005. **41**(2): p. 143-151.

56. Willems, G., et al., *A classification of dental composites according to their morphological and mechanical characteristics.* Dental Materials, 1992. **8**(5): p. 310-319.

57. Desai, S., et al., *Fibrous micro-composite material*. 2008, Google Patents.

58. Bisegna, P. and R. Luciano, *On methods for bounding the overall properties of periodic piezoelectric fibrous composites.* Journal of the Mechanics and Physics of Solids, 1997. **45**(8): p. 1329-1356.

59. Advani, S.G. and C.L. Tucker III, *The use of tensors to describe and predict fiber orientation in short fiber composites.* Journal of rheology, 1987. **31**(8): p. 751-784.

60. Shen, H. and S. Nutt, *Mechanical characterization of short fiber reinforced phenolic foam.* Composites Part A: Applied science and manufacturing, 2003. **34**(9): p. 899-906.

61. Lee, Y., et al., *Characterization of fiber orientation in short fiber reinforced composites with an image processing technique.* Materials Research Innovations, 2002. **6**(2): p. 65-72.

62. Ivey, M., et al., *Characterizing short-fiber-reinforced composites produced using additive manufacturing.* Advanced Manufacturing: Polymer & Composites Science, 2017. **3**(3): p. 81-91.

63. De Rosa, I.M., C. Santulli, and F. Sarasini, *Mechanical and thermal characterization of epoxy composites reinforced with random and quasi-unidirectional untreated Phormium tenax leaf fibers.* Materials & Design (1980-2015), 2010. **31**(5): p. 2397-2405.

64. Wang, J., et al., *Experimental fabrication and characterization of out-of-plane fiber waviness in continuous fiber-reinforced composites.* Journal of Composite Materials, 2012. **46**(17): p. 2041-2053.

65. Kumar, S., et al., *Development and characterization of polymer–ceramic continuous fiber reinforced functionally graded composites for aerospace application.* Aerospace Science and Technology, 2013. **26**(1): p. 185-191.

66. Hao, W., et al., *Preparation and characterization of 3D printed continuous carbon fiber reinforced thermosetting composites.* Polymer Testing, 2018. **65**: p. 29-34.

67. Tracy, J., S. Daly, and K. Sevener, *Multiscale damage characterization in continuous fiber ceramic matrix composites using digital image correlation.* Journal of Materials Science, 2015. **50**(15): p. 5286-5299.

68. Devendra, K. and T. Rangaswamy, *Strength characterization of E-glass fiber reinforced epoxy composites with filler materials.* Journal of Minerals and Materials Characterization and Engineering, 2013. **1**(6): p. 353-357.

69. Sato, N., et al., *Microfailure behaviour of randomly dispersed short fibre reinforced thermoplastic composites obtained by direct SEM observation.* Journal of Materials Science, 1991. **26**(14): p. 3891-3898.

70. Fu, S.-Y., et al., *Tensile properties of short-glass-fiber-and short-carbon-fiber-reinforced polypropylene composites.* Composites Part A: Applied Science and Manufacturing, 2000. **31**(10): p. 1117-1125.

71. Ning, F., et al., *Additive manufacturing of carbon fiber reinforced thermoplastic composites using fused deposition modeling.* Composites Part B: Engineering, 2015. **80**: p. 369-378.

72. Tekinalp, H.L., et al., *Highly oriented carbon fiber–polymer composites via additive manufacturing.* Composites Science and Technology, 2014. **105**: p. 144-150.

73. Karapappas, P., et al., *Enhanced fracture properties of carbon reinforced composites by the addition of multi-wall carbon nanotubes.* Journal of Composite Materials, 2009. **43**(9): p. 977-985.

74. Blok, L.G., et al., *An investigation into 3D printing of fibre reinforced thermoplastic composites.* Additive Manufacturing, 2018. **22**: p. 176-186.

75. Zhong, W., et al., *Short fiber reinforced composites for fused deposition modeling.* Materials Science and Engineering: A, 2001. **301**(2): p. 125-130.

76. Quan, Z., et al., *Additive manufacturing of multi-directional preforms for composites: opportunities and challenges.* Materials Today, 2015. **18**(9): p. 503-512.

77. Ning, F., et al., *Additive manufacturing of carbon fiber-reinforced plastic composites using fused deposition modeling: effects of process parameters on tensile properties.* Journal of Composite Materials, 2017. **51**(4): p. 451-462.

78. Compton, B.G., et al., *Direct-write 3D printing of NdFeB bonded magnets.* Materials and Manufacturing Processes, 2018. **33**(1): p. 109-113.

79. Hmeidat, N.S., J.W. Kemp, and B.G. Compton, *High-strength epoxy nanocomposites for 3D printing.* Composites Science and Technology, 2018. **160**: p. 9-20.

80. Hayes, S., et al., *A self-healing thermosetting composite material.* Composites Part A: Applied Science and Manufacturing, 2007. **38**(4): p. 1116-1120.

81. Pierson, H., et al., *Mechanical properties of printed epoxy-carbon fiber composites.* Experimental Mechanics, 2019: p. 1-15.

82. Compton, B.G. and J.A. Lewis, *3D printing: 3d-printing of lightweight cellular composites (Adv. Mater. 34/2014).* Advanced Materials, 2014. **26**(34): p. 6043-6043.

83. Johnson, K.J., et al., *In operando monitoring of dynamic recovery in 3D-printed thermoset nanocomposites by XPCS.* Langmuir, 2019. **35**(26): p. 8758-8768.

84. Pierson, H., et al., *Mechanical properties of printed epoxy-carbon fiber composites.* Experimental Mechanics, 2019. **59**(6): p. 843-857.

85. Chandrasekaran, S., et al., *3D printing of high performance cyanate ester thermoset polymers.* Journal of Materials Chemistry A, 2018. **6**(3): p. 853-858.

86. Wu, T., et al., *Additively manufacturing high-performance bismaleimide architectures with ultraviolet-assisted direct ink writing.* Materials & Design, 2019. **180**: p. 107947.

87. Lewicki, J.P., et al., *3D-printing of meso-structurally ordered carbon fiber/polymer composites with unprecedented orthotropic physical properties.* Scientific Reports, 2017. **7**(1): p. 1-14.

88. Karsli, N.G. and A. Aytac, *Tensile and thermomechanical properties of short carbon fiber reinforced polyamide 6 composites.* Composites Part B: Engineering, 2013. **51**: p. 270-275.

89. Invernizzi, M., et al., *UV-assisted 3D printing of glass and carbon fiber-reinforced dual-cure polymer composites.* Materials, 2016. **9**(7): p. 583.

90. Lewicki, J., et al., *Additive manufacturing continuous filament carbon fiber epoxy composites*. 2017, Google Patents.

91. Jing, W., et al., *Surface modification of carbon fibers and the selective laser sintering of modified carbon fiber/nylon 12 composite powder.* Materials & Design, 2017. **116**: p. 253-260.

92. Spowart, J.E., N. Gupta, and D. Lehmhus, *Additive manufacturing of composites and complex materials.* Jom, 2018. **70**(3): p. 272-274.

93. Peroni, L., et al., *Dynamic mechanical behavior of syntactic iron foams with glass microspheres.* Materials Science and Engineering: A, 2012. **552**: p. 364-375.

94. Santa Maria, J.A., et al., *Effect of hollow sphere size and size distribution on the quasi-static and high strain rate compressive properties of Al-A380–Al2O3 syntactic foams.* Journal of Materials Science, 2014. **49**(3): p. 1267-1278.

95. Avalle, M., et al., *AlSi7 metallic foams–aspects of material modelling for crash analysis.* International Journal of Crashworthiness, 2009. **14**(3): p. 269-285.

96. Dou, Z., et al., *High strain rate compression of cenosphere-pure aluminum syntactic foams.* Scripta Materialia, 2007. **57**(10): p. 945-948.

97. Singh, A.K., et al., *Additive manufacturing of syntactic foams: part 1: development, properties, and recycling potential of filaments.* Jom, 2018. **70**(3): p. 303-309.

98. Singh, A.K., et al., *Additive manufacturing of syntactic foams: part 2: specimen printing and mechanical property characterization.* Jom, 2018. **70**(3): p. 310-314.

99. Singh, A.K., et al., *Additive manufacturing of three-phase syntactic foams containing glass microballoons and air pores.* Jom, 2019. **71**(4): p. 1520-1527.

100. Patil, B., B.R. Bharath Kumar, and M. Doddamani, *Compressive behavior of fly ash based 3D printed syntactic foam composite.* Materials Letters, 2019. **254**: p. 246-249.

101. Peroni, L., et al., *Investigation of the mechanical behaviour of AISI 316L stainless steel syntactic foams at different strain-rates.* Composites Part B: Engineering, 2014. **66**: p. 430-442.

102. Salvo, L., et al., *Processing and structures of solids foams.* Comptes Rendus Physique, 2014. **15**(8-9): p. 662-673.

103. Gupta, N. and R. Nagorny, *Tensile properties of glass microballoon-epoxy resin syntactic foams.* Journal of Applied Polymer Science, 2006. **102**(2): p. 1254-1261.

104. Kumar, B.B., et al., *Processing of cenosphere/HDPE syntactic foams using an industrial scale polymer injection molding machine.* Materials & Design, 2016. **92**: p. 414-423.

105. Aureli, M., M. Porfiri, and N. Gupta, *Effect of polydispersivity and porosity on the elastic properties of hollow particle filled composites.* Mechanics of Materials, 2010. **42**(7): p. 726-739.

106. Tagliavia, G., M. Porfiri, and N. Gupta, *Analysis of flexural properties of hollow-particle filled composites.* Composites Part B: Engineering, 2010. **41**(1): p. 86-93.

107. Delta Bot Hackka 3D Printer: https://all3dp.com/1/anycubic-kossel-linear-plus-3d-printer-review-delta/.

108. Thinky (AR-310) Mixer: https://www.thinkymixer.com/en-us/

109. Universal Instron Machine: https://www.instron.us/en-us/products/testing-systems/universal-testing-systems/.

110. Anderson, T.L., *Fracture mechanics: fundamentals and applications*. 2017: CRC press.

111. Van Hattum, F. and C. Bernardo, *A model to predict the strength of short fiber composites.* J Polymer composites, 1999. **20**(4): p. 524-533.

112. Ashby, M.F., *Materials Selection in Mechanical Design, 4th Ed*. 2011, Burlington, MA, USA: Elsevier.

113. Van de Werken, N., et al., *Investigating the effects of fiber surface treatment and alignment on mechanical properties of recycled carbon fiber composites.* Composites Part A: Applied Science and Manufacturing, 2019. **119**: p. 38-47.

114. Callister, W.D. and D.G. Rethwisch, *Materials Science and Engineering*. Vol. 5. 2011: John wiley & sons NY.

115. Obaid, N., M.T. Kortschot, and M. Sain, *Predicting the stress relaxation behavior of glass-fiber reinforced polypropylene composites.* Composites Science and Technology, 2018. **161**: p. 85-91.

116. Szymczyk, E., J. Jachimowicz, and K. Puchała, *Analysis of load transfer into composite structure.* Applied Computer Science, 2014. **10**(3).

117. Sasikala, L., R. Rathinamoorthy, and B. Durai, *Effect of fibre composition on essential properties of needle-punched nonwoven fabrics as secondary layer for composite wound dressings.* Indian Journal of Fibre & Textile Research (IJFTR), 2019. **44**(2): p. 148-154.

118. Kevlar Continious Fibers: https://store.acpsales.com/products/2336/aramid-uni-web-unidirectional-fiber.

119. Compton, B.G. and J.A. Lewis, *3D-printing of lightweight cellular composites.* Advanced Materials, 2014. **26**(34): p. 5930.

120. Wang, K., et al., *Flexure behaviors of ABS-based composites containing Carbon and Kevlar fibers by material extrusion 3D printing.* Polymers, 2019. **11**(11).

121. Rizzi, E., E. Papa, and A. Corigliano, *Mechanical behavior of a syntactic foam: experiments and modeling.* International Journal of Solids and Structures, 2000. **37**(40): p. 5773-5794.

122. Yu, W., H. Xue, and M. Qian, *Tensile and compressive properties of epoxy syntactic foams reinforced by short glass fiber.* 2017.

123. Fleck, N.A., V.S. Deshpande, and M.F. Ashby, *Micro-architectured materials: past, present and future.* Proceedings of the Royal Society A-Mathematical Physical and Engineering Sciences, 2010. **466**(2121): p. 2495-2516.